NASA CR114632

STUDY OF CO_2 SORBENTS FOR EXTRAVEHICULAR ACTIVITY

July 1973

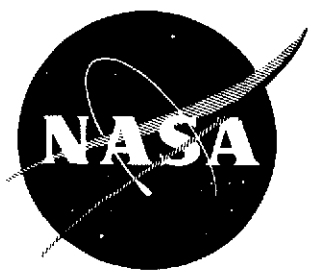

Prepared under Contract No. NAS2-6959
by McDonnell Douglas Astronautics Company
Huntington Beach, California
for
NATIONAL AERONAUTICS AND SPACE ADMINISTRATION

STUDY OF CO_2 SORBENTS FOR EXTRAVEHICULAR ACTIVITY

July 1973

PREPARED BY:
G. V. COLOMBO
SENIOR ENGINEER/SCIENTIST
BIOTECHNOLOGY AND POWER
RESEARCH AND DEVELOPMENT

APPROVED BY:
K. H. HOUGHTON, M.D.
CHIEF ENGINEER
BIOTECHNOLOGY AND POWER
RESEARCH AND DEVELOPMENT

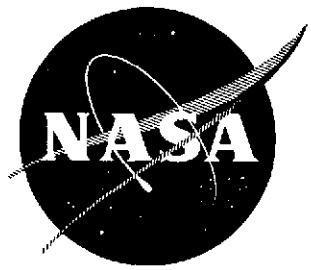

Prepared under Contract No. NAS2-6959
by McDonnell Douglas Astronautics Company
Huntington Beach, California
for
NATIONAL AERONAUTICS AND SPACE ADMINISTRATION

PREFACE

This report, Study of CO_2 Sorbents for Extravehicular Activity, was prepared by McDonnell Douglas Astronautics Company for the Ames Research Center, National Aeronautics and Space Administration, Moffett Field, California, under Contract No. NAS2-6959. Acknowledgment is given Mr. Mark Leban, Technical Monitor, ARC, for his direction of the study effort.

CONTENTS

FIGURES

TABLES

Section 1

INTRODUCTION AND SUMMARY

Future manned space exploration missions will include requirements for frequent extravehicular activity (EVA) sorties. In order to meet these requirements efficiently, studies have shown that portable life support equipment must be provided for the astronauts which is capable of repeated use as well as regeneration between sorties. In anticipation of these requirements, NASA Ames Research Center has completed studies of Advance Extravehicular Protective Systems (AEPS), References 1 and 2. The results of these studies have indicated that the critical areas for research effort are (1) the development of regenerable thermal storage devices to which the heat generated by the suited astronaut and his equipment could be rejected and (2) a regenerable CO_2 removal subsystem for purifying the recycled breathing gas of the of the astronaut. The most promising methods for performing the CO_2 removal function were identified as metallic oxides and/or metallic hydroxides. A schematic of a representative system is shown in Figure 1-1.

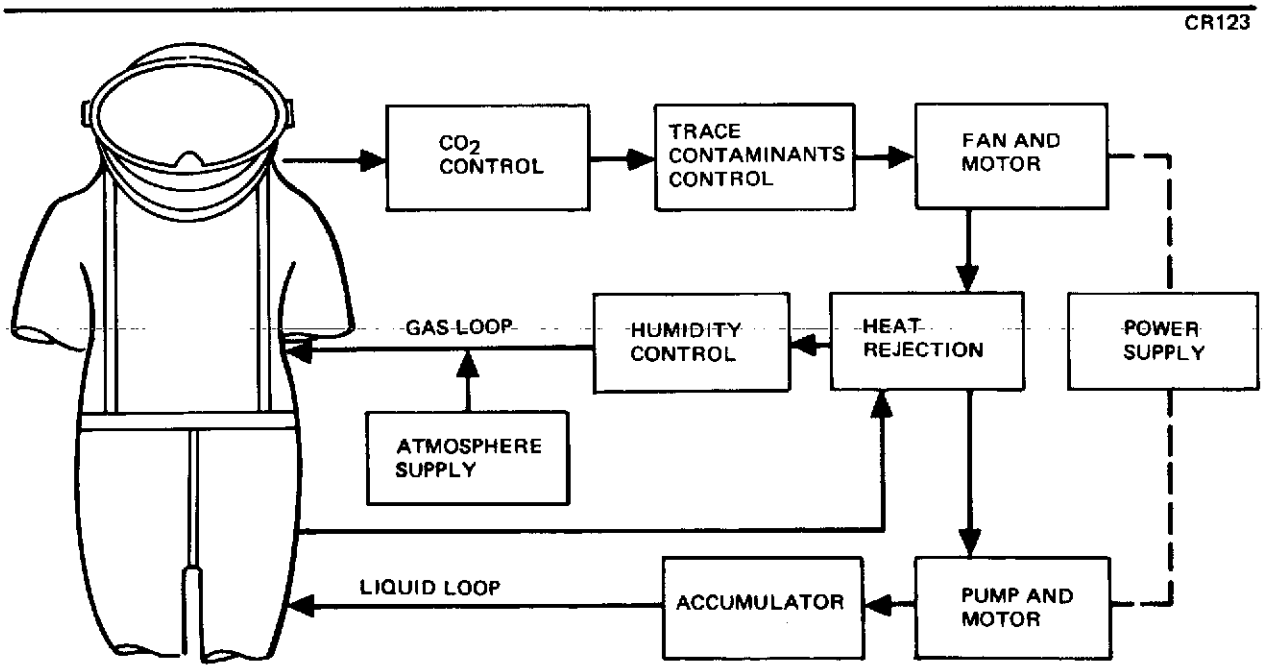

Figure 1-1. Representative Functional Schematic of EV Life Support System

This program provides an experimental and analytical study of the use of the metallic oxides – MgO, Ag_2O, and ZnO – and metallic hydroxides – $Mg(OH)_2$ and $Zn(OH)_2$. Measurements of sorption and regeneration properties of each material were obtained with various methods of material fabrication and formulations evaluated. The hydroxides of magnesium and zinc were found to exhibit essentially no affinity for CO_2 and were not regenerable. Zinc oxide compounds showed poor affinity for CO_2, and a stable structural form could not be found. A binder system was developed which produced very strong pellets of magnesium oxide; however, its CO_2 sorption capacity could not be improved over previous levels, as reported in Reference 3.

A silver oxide formulation was developed which rapidly absorbs approximately 95 percent of its 0.19 Kg CO_2/Kg oxide and has shown no sorption or structural degradation through 22 regenerations. It is recommended that this basic formula be developed further and tested in large-scale beds under simulated AEPS conditions.

Section 2

TECHNICAL PROGRAM

The objective of this program was to select the most promising candidate material for development as a regenerable CO_2 sorbent for EVA. This was accomplished by manufacturing pellets from the candidate materials containing various additives and evaluating their CO_2 sorption capacities under fixed conditions. Detailed chemical and physical analyses of the most promising candidates were conducted in an effort to characterize properties which were conducive to desirable performance. Studies of the regeneration processes were also conducted.

2.1 THEORETICAL CONSIDERATIONS

The NASA-sponsored AEPS studies (References 1 and 2) not only identified the requirements for regenerable CO_2 sorption materials but also identified some of the more promising candidates. Table 2-1 lists the general performance requirements dictated by some of the most likely mission profiles identifiable to date. These are quite ambitious compared to the Apollo requirements, also shown in the table.

The most promising approach to the development of a high-capacity, regenerable CO_2 sorbent identified by the AEPS studies is the ability of some metallic oxides to react with CO_2 to form the metallic carbonate according to the reaction:

$$MO + CO_2 \rightleftarrows MCO_3$$

This reaction is reversible at elevated temperatures, thus thermally decomposing the carbonate, liberating CO_2, and reforming the oxide.

Table 2-2 lists the properties of interest of the metals comprising Groups I and II of the Periodic Table of Elements. The most attractive metal from

Table 2-1
EVA MISSION REQUIREMENTS PARAMETERS

Mission	EVA Duration (hr)	Average Metabolic Rate		Carbon Dioxide Partial Pressure				Number of EVA's	Resupply Period (days)
				Nominal		Maximum			
		$J \times 10^6$	Btu/hr	N/m^3	mm Hg	N/m^3	mm Hg		
Space Station[1]	4	1.05	1,000	532	4	998	7.5	500	90
Lunar Base[1]	8	1.11	1,050	532	4	998	7.5	500	180
Mars[1]	8	1.27	1,200	532	4	998	7.5	22	None
Shuttle[1]	4	1.05	1,000	532	4	998	7.5	600	7
Space Station Emergency System[1]	1/2	1.59	1,500	-	-	1,999	15	-	90
Lunar Base Emergency System[1]	2	1.69	1,600	-	-	1,999	15	-	180
Mars Emergency System[1]	1	2.21	2,000	-	-	1,999	15	-	None
Shuttle Emergency System[1]	1/2	1.59	1,500	-	-	1,999	15	-	7
Apollo 15 through 17[2]	6	1.27	1,200	-	-	-	15	-	-

[1] References 1, 2

[2] Reference 4

Table 2-2

THERMAL AND MASS CAPACITY EVALUATION FOR METALLIC OXIDES

Metallic Oxide	(Kg/m^3)	(Weight %)	Regeneration Energy ($J/Kg \times 10^6$)
Group IA			
Li_2O	2,013	147	5.13
Na_2O	2,270	71	7.30
K_2O	2,320	47	8.87
Rb_2O	3,720	24	9.13
Cs_2O	4,360	16	9.25
Group IB			
Ag_2O	7,143	19	1.86
Au_2O	3,600	11	-
Group IIA			
BeO	3,010	176	-
MgO	3,580	110	2.68
CaO	3,370	28	4.03
SrO	4,700	42	5.34
BaO	5,670	29	6.06
Group IIB			
CdO	7,000	34	2.26
ZnO	5,470	54	1.61

the standpoint of potential CO_2 capacity is magnesium, which also has one of the lower regeneration energy requirements. Zinc and silver are attractive because of extremely low energy requirements. Easily eliminated are beryllium and cadmium because they are toxic, and lithium oxide due to its explosive instability in the presence of moisture. Early work with MgO (Reference 3) indicated the importance of a high moisture content in the reaction between MgO and CO_2. A postulated reaction mechanism of (Reference 1):

$$MgO + H_2O \rightleftharpoons Mg(OH)_2$$

$$Mg(OH)_2 + CO_2 \rightleftharpoons MgCO_3 + H_2O$$

led to the selection of $Mg(OH)_2$ and $Zn(OH)_2$ as additional candidate materials (AgOH) does not exist). The theoretical CO_2 sorption capacities of the five candidate materials are listed in Table 2-3.

Figure 2-1 shows the equilbrium behavior of the three metallic carbonates. It should be noted that these materials behave differently than the more commonly encountered CO_2 adsorbents. The CO_2 partial pressure in equilbrium with the metal oxide is solely dependent on temperature and independent of bed loading as long as any oxide is in contact with the atmosphere.

Figure 2-2 shows the equilibrium behavior of the two metal hydroxides in addition to the carbonates. In both cases the hydroxides decompose well below the carbonates, thus direct regeneration of a hydroxide sorbent is not possible unless the vapor pressure of water is maintained above the equilibrium point. This is feasible with $Zn(OH)_2$ but the pressures required by $Mg(OH)_2$ would be much too high to be practical. The only alternate regeneration process is to decompose the carbonate to the oxide and then hydrate the oxide to the hydroxide with water; however, literature sources show that this does not occur to any appreciable extent and the extensive commercial use of magnesia ceramics substantiates this fact.

Table 2-3

THEORETICAL CO_2 CAPACITIES OF CANDIDATE METALLIC OXIDES AND HYDROXIDES

Candidate	Weight Percent CO_2 Capacity
MgO	1.092
$Mg(OH)_2$	0.760
ZnO	0.540
$Zn(OH)_2$	0.443
Ag_2O	0.189

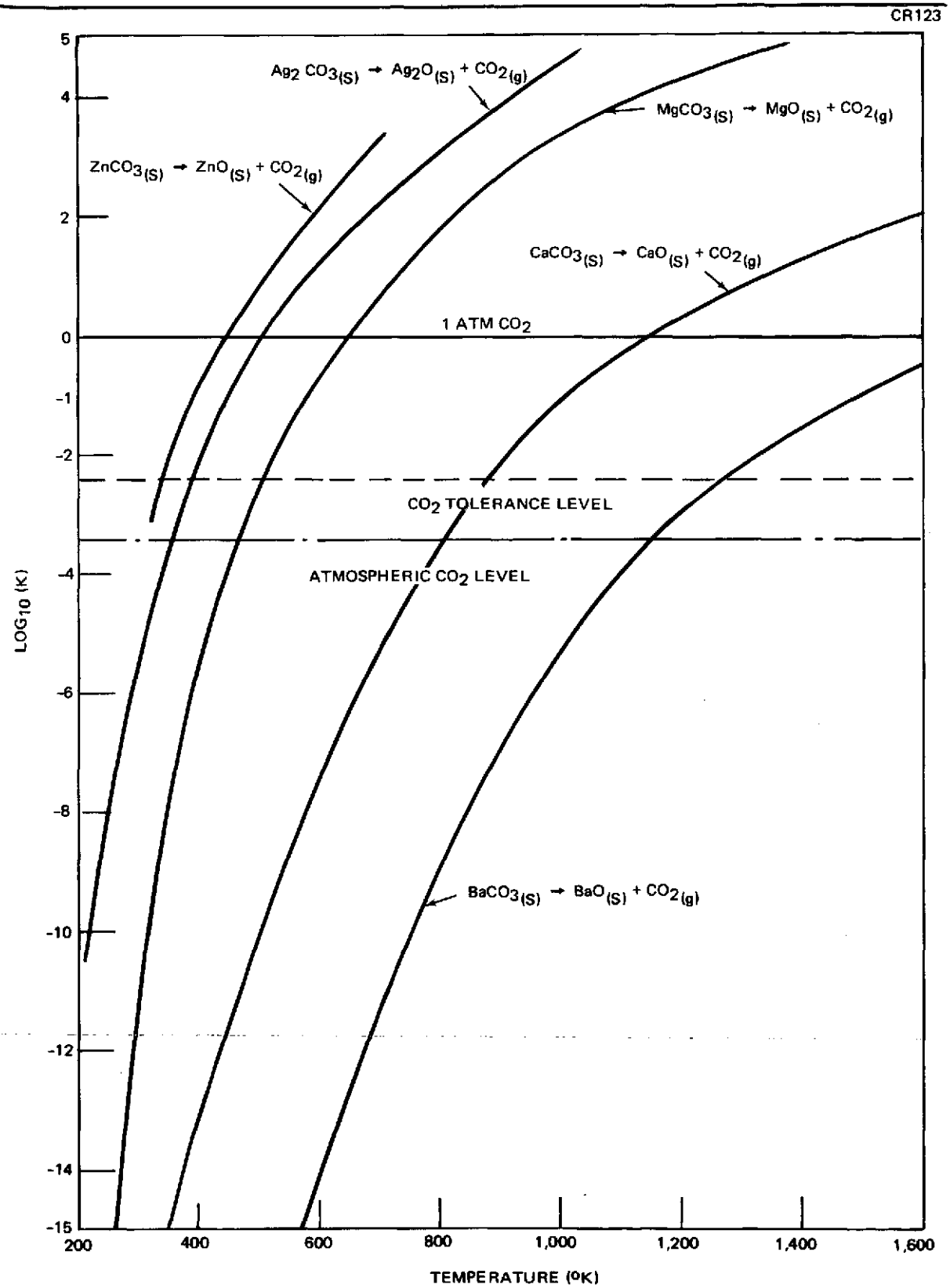

Figure 2-1. Decomposition Temperatures of Metal Carbonates

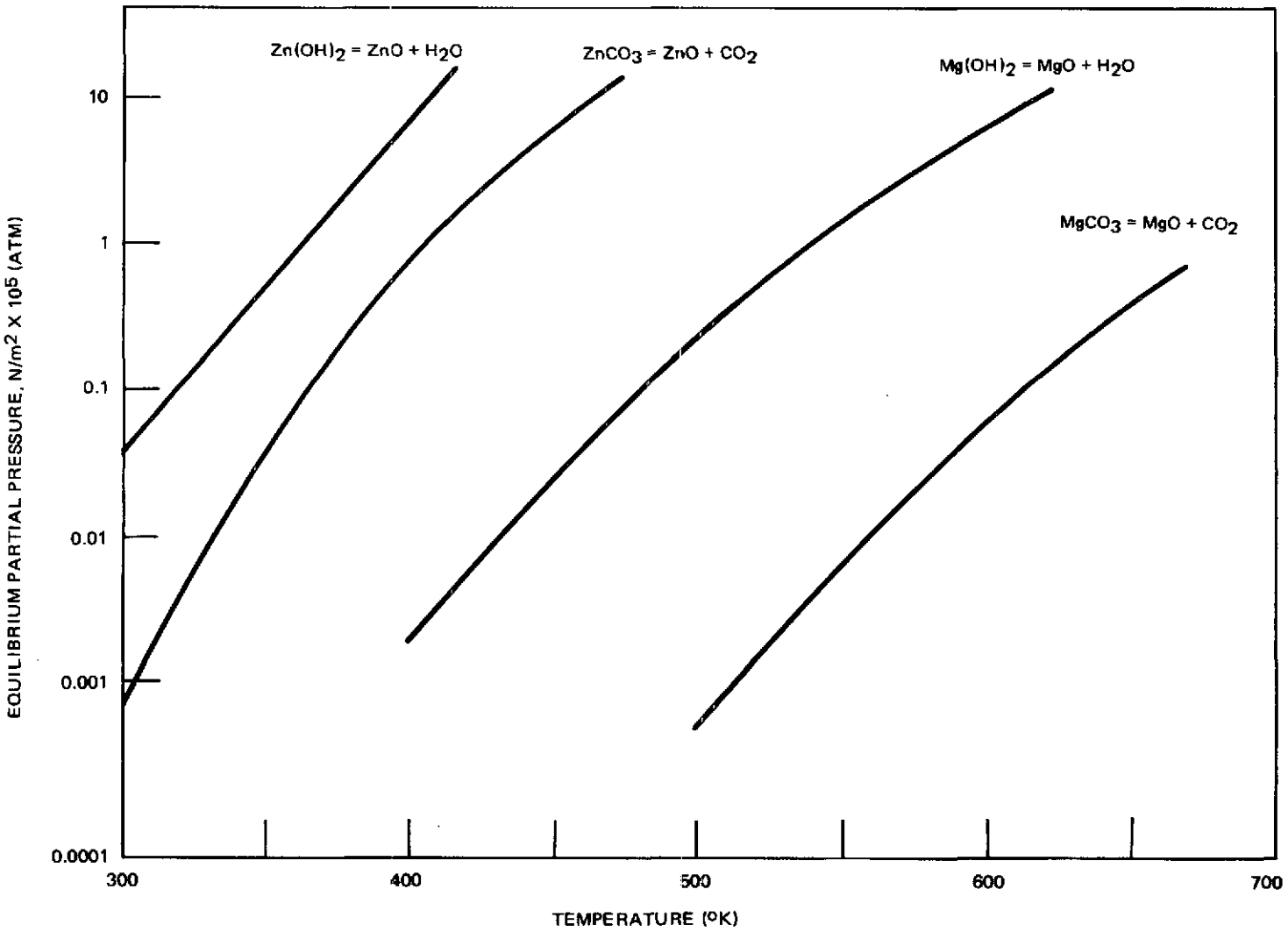

Figure 2-2. Equilibrium for Metallic Carbonates and Hydroxides

2.2 MATERIAL PREPARATION

The selection of the most promising candidate material was accomplished by manufacturing pellets similar to the configuration in which they would be used in an operational system, and evaluating their performance under identical conditions.

2.2.1 Preparation of Oxides

Previous studies (References 3 and 5) have shown that an oxide most suitable for reaction with CO_2 is formed from freshly decomposed carbonate. Consequently, all pellets were manufactured in the carbonate form and then thermally converted to the oxide. Pure oxide pellets were manufactured from AR-grade metal carbonate in a water slurry. The addition of catalysts and binders was accomplished before the pellets were made. The most widely used additives were alkali metal hydroxides and sodium silicate. Aqueous solutions of these additives were thoroughly dispensed through the carbonate powder in a mortar and pestle before loading into the pellet maker.

2.2.2 Preparation of Hydroxides

Commercial sources of $Mg(OH)_2$ and $Zn(OH)_2$ could not be located; consequently, they were manufactured by precipitation from alkaline solutions.

One-tenth kilogram of $Mg(OH)_2$ was manufactured by adding a solution of 0.440 Kg $Mg(NO_3)_2 \cdot 6H_2O$ in 500 μm^3 of water dropwise to a solution of 0.203 Kg KOH in 600 μm^3 H_2O. The resulting precipitate was gelatinous and extremely difficult to filter. The precipitate was resuspended twice in 400 μm^3 of water and dried at 358°K.

One-tenth kilograph of $Zn(OH)_2$ was manufactured by adding a 0.300 Kg $Zn(NO_3)_2 \cdot 6H_2O$ in 1,000 μm^3 solution dropwise to 0.085 Kg NaOH in 400 μm^3 of H_2O. The resulting precipitate was resuspended twice in 600 μm^3 of H_2O and dried at 358°K.

2.2.3 Pellet Manufacture

The materials were formed into pellets using the device shown in Figure 2-3. The pellets were produced by extrusion of a slurry on a moving belt which is dried with hot air. The test material in slurry form was loaded into a hopper

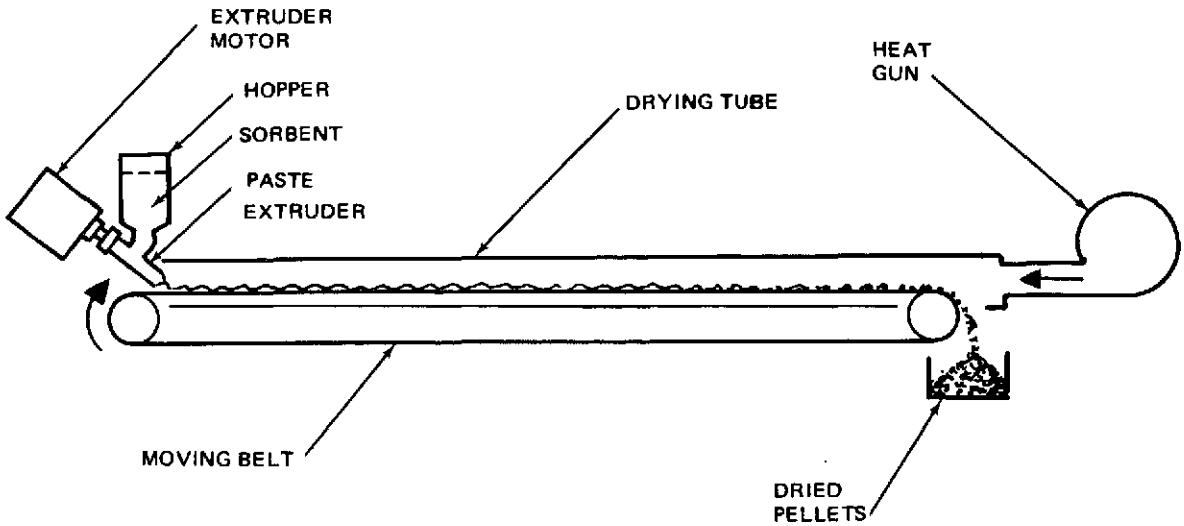

Figure 2-3. Pellet Maker

and forced through a nozzle by a piston-type slurry pump. The belt passed through a 0.05-m square aluminum tube 2 m long through which hot air was forced counter-currently by a heat gun. Thus, the pellets were partially dried as they passed through the tube and easily fell off the belt as it passed over the end roller.

2..2.4 Activation

The newly manufactured pellets were dried overnight at 355°K. Activation was accomplished in a muffle furnace at a temperature sufficient to decompose the carbonate to oxide. These temperatures were determined by measuring the weight loss from samples of pure carbonate after one-hour exposure in the furnace at increasing increments of 25°K. Magnesium carbonate was found to equilibrate after one hour at 723°K while both zinc and silver carbonates required only 523°K. All pellets were activated by placing them in an alumina crucible and placing it in a preheated furnace at the appropriate temperature for two hours. Cooling was accomplished by placing the crucible in a dessicator. This procedure was also used when multiple regenerations of a material were accomplished.

2.2.5 Pre-Wetting

Early work with magnesium oxide (Reference 3) showed that significant improvements in sorption rates and capacities could be accomplished by adding moisture in amounts from 10 to 100 percent of the dry weight of the bed. This was accomplished by exposing the pellets to saturated steam. The apparatus used is shown in Figure 2-4. A wire basket containing the pellets was suspended from a balance in a chamber through which saturated steam was passed. Thus, the weight change from the added moisture could be followed and the process stopped when the desired loading was achieved. The method provided a consistent moisture content throughout the bed since the pellets formed a shallow layer in the bottom of the basket.

2.3 TEST APPARATUS

The candidate materials were compared by obtaining CO_2 breakthrough curves under identical test conditions. The regeneration characteristics of the most promising candidate were determined by monitoring the CO_2 evolution as a function of time. The crush strengths of all candidate pellets were also measured.

2.3.1 Screening Test Apparatus

The apparatus used in the screening tests is shown in Figure 2-5. The candidate sorbent material pellets were placed in a 0.025-m diameter glass tube filled to a depth of approximately 0.1 m. This bed configuration was found to yield reliable data without appreciable channeling or wall effects. The tube was then mounted vertically (the pellets supported by a layer of glass beads) and connected to the flow apparatus. A humidified stream of 1.1 percent CO_2 in nitrogen, simulating the maximum expected feed concentration, was fed to the tube at a rate of 200 μm^3/min. Experience has shown that the use of certified gas mixtures provides consistent and reliable feed compositions. The effluent from the tube was continuously monitored for CO_2 concentration with an MSA Model 300 infrared analyzer calibrated at 1.1 percent CO_2 full scale. Continuous water concentration was monitored by a Cambridge Model 880 Dewpointer. The readouts from these two instruments were recorded continuously on strip chart recorders.

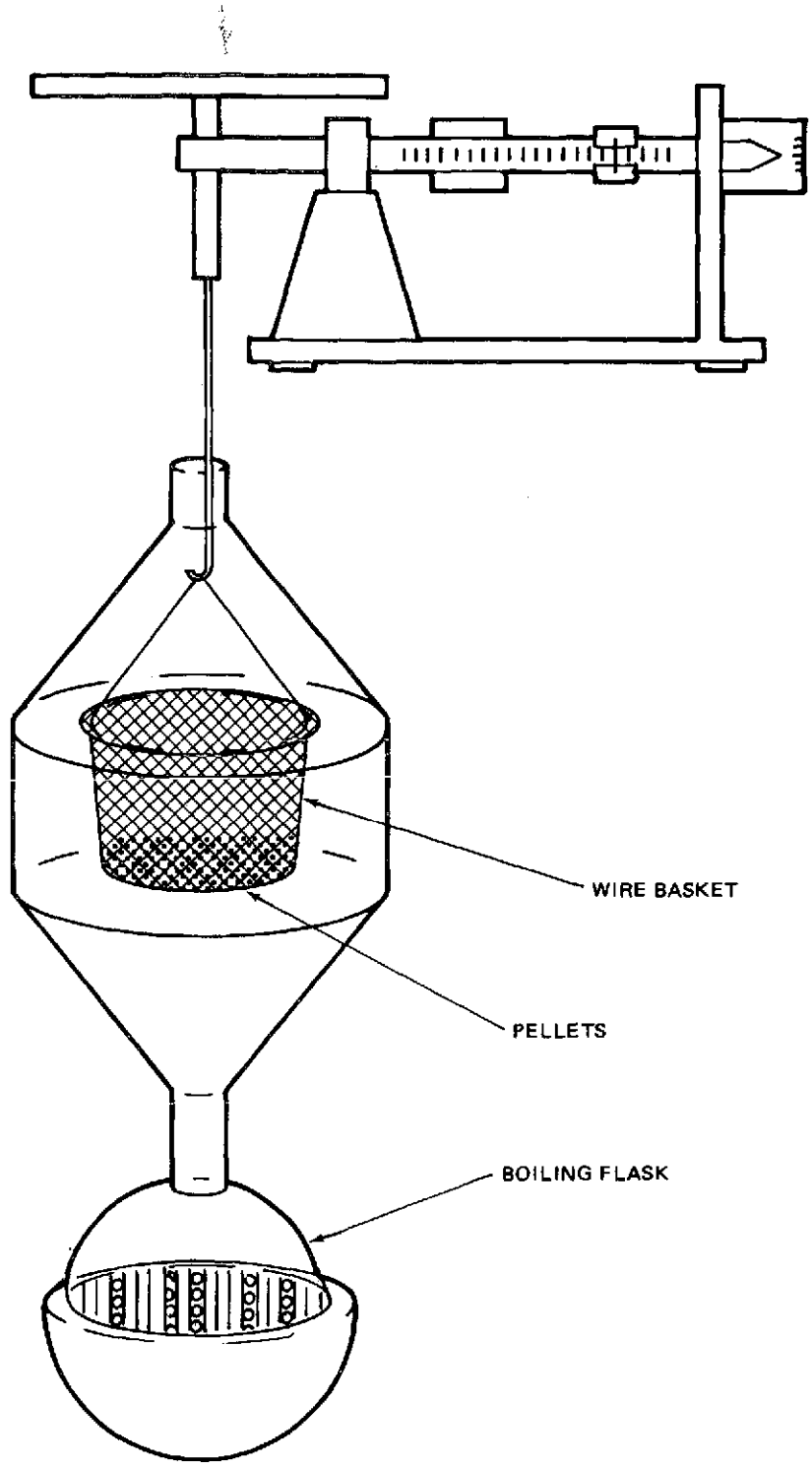

Figure 2-4. Pellet Steamer

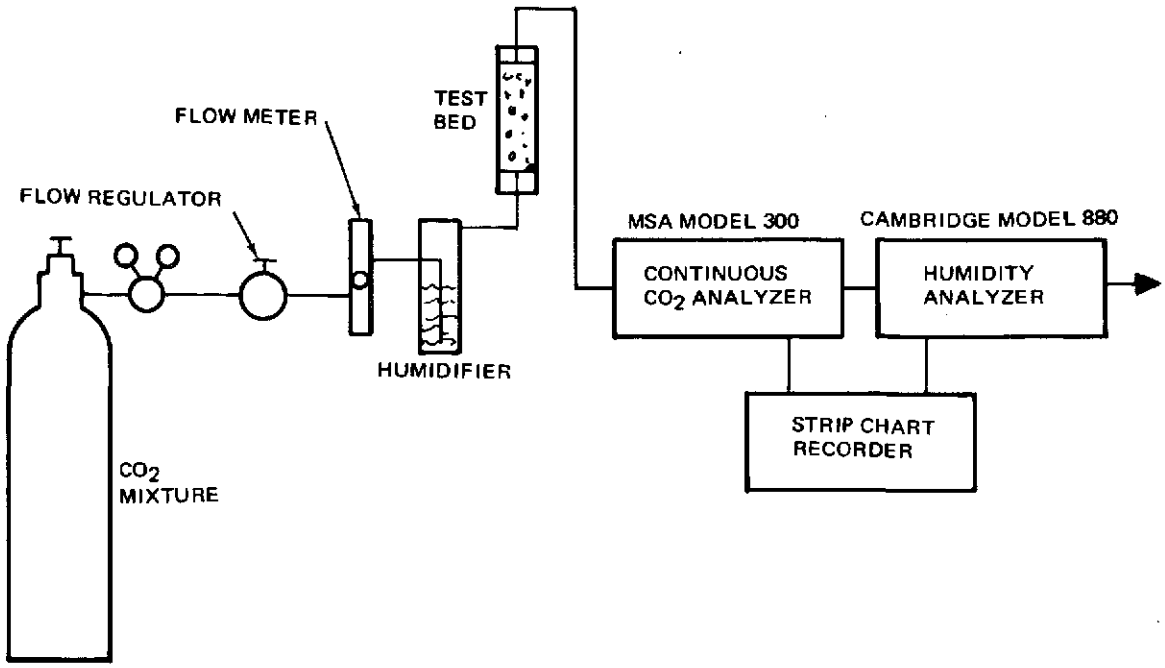

Figure 2-5. Preliminary Screening Test Apparatus

2.3.2 Regeneration Test Apparatus

The regeneration characteristics of the materials were studied using the apparatus shown in Figure 2-6. The pellets were contained in the same glass tube used for the sorption process. This tube fit inside a copper tube which in turn was placed in an electric combustion tube furnace. A thermocouple soldered to the copper tube was connected to a recorder/controller which controlled the tube temperature and provided a time/temperature curve. An auxiliary thermocouple was placed in the center of the bed to provide core temperatures. In most cases, a stream of dry nitrogen was passed through the bed to carry the evolved moisture and CO_2. A condenser/collector was provided at the exit to quantitatively collect evolved moisture. A Beckman GC2-A gas chromatograph was provided to measure the CO_2 concentration of the exit stream at 4-minute intervals, thus providing a CO_2 evolution curve. In some cases, a diaphragm vacuum pump was placed between the condenser and gas chromatograph to simulate conditions which might be used in a regeneration system which recovers the CO_2. In one case, a Welch roughing pump was connected upstream of the condenser and the nitrogen purge was stopped to simulate regeneration to space.

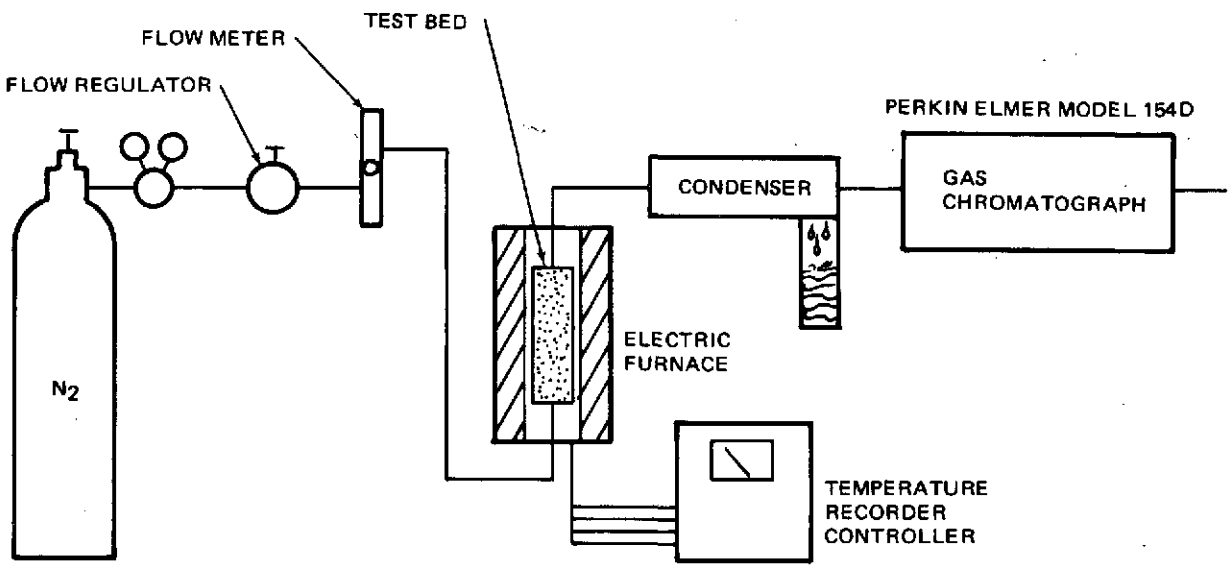

Figure 2-6. Metallic Oxide Regeneration Test Apparatus

2.3.3 Pellet Crush Strength Tester

The device shown in Figure 2-7 was used to measure the crush strength of all pellets manufactured. A pneumatic cylinder with a known cross section piston was connected to a pressure gage and pressure regulator. The test pellet was placed below the piston shaft and the pressure increased until the pellet fractured. The indicated pressure was then used to calculate the force required to crush the pellet.

2.4 SCREENING RESULTS

The results of the preliminary screening tests are presented later in this section in Tables 2-4 through 2-9. The sample nomenclature has been assigned as follows. The first letter designates the parent oxide, i.e., M for magnesium, Z for zinc, and S for silver. The number following the first letter designates the serial number of the composition of this particular compound. The third digit is either a D or W denoting whether the sample was first tested dry or with water added. The fourth digit denotes whether the sample was tested again wet or dry, or the number of times this sample

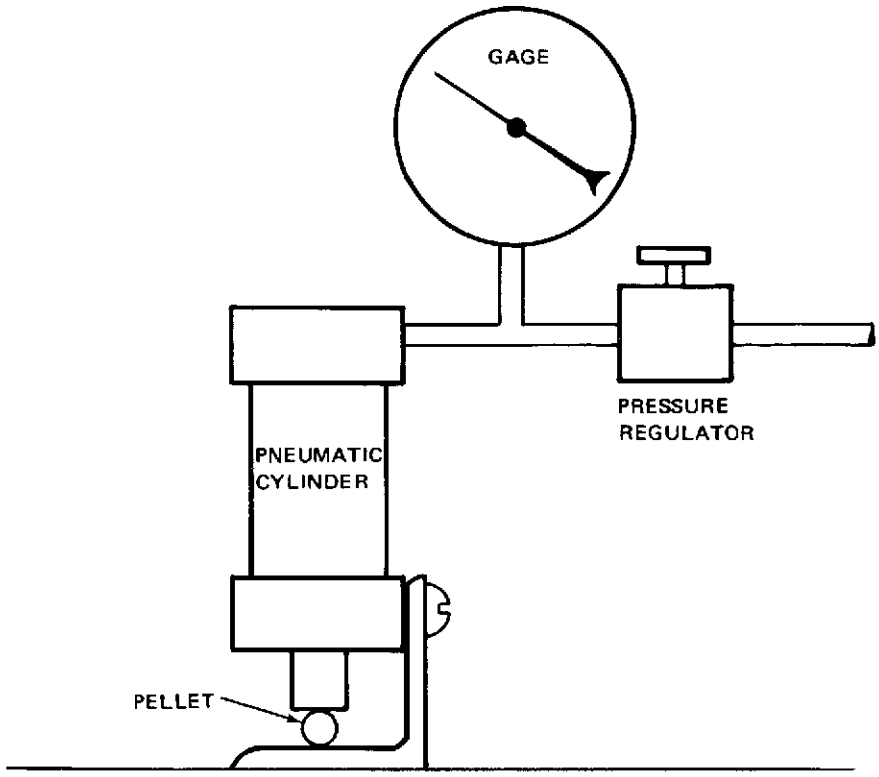

Figure 2-7. Pellet Crush Strength Test Apparatus

has been regenerated. For example, sample Z2D2 is the second zinc compound to be manufactured and it has been regenerated and tested dry twice. Sample M6DW2 is the sixth magnesium compound. It was first tested dry, then tested wet twice.

The first columns in the tables give the sample composition in the as-tested form. All samples tested were manufactured using the parent metal in the carbonate form, and then regenerating to the oxide in a furnace. Magnesium samples were regenerated at 723°K, and zinc and silver at 523°K. Weight reduction factors of 0.48 Kg MgO/Kg $MgCO_3$, 0.74 Kg ZnO/ Kg $ZnCO_3$ and 0.84 Kg Ag_2O/Kg Ag_2CO_3, and 0.47 Kg Na_2SiO_3/Kg 42° Be Na_2SiO_3 solution were determined experimentally. These factors differ from theoretical conversions from the carbonates and indicate that the carbonates used as starting materials contain appreciable amounts of the oxides. Regenerations were carried well past the theoretical temperature in these determinations to ensure complete degradation.

The second column in the tables lists the weight of the sample in the screening tests and includes the added moisture in the W samples. The BT time in column 3 is the time in minutes before CO_2 first appeared in the bed effluent. The "time to 80%" is the time required for the CO_2 concentration in the effluent to reach approximately 80 percent of the feed concentration.

The "wt % CO_2 at BT" column is the weight of CO_2 absorbed by the bed up to the time of breakthrough expressed as a percent of the initial bed weight, and the "wt % CO_2 at 80%" is the weight of CO_2 absorbed when the effluent concentration of CO_2 reaches 80 percent of the feed concentration.

The bed depth column is included since some of the earlier tests were conducted with large beds before the 0.1 m bed depth was selected as a standard. The ρCO_2 column expresses the weight of CO_2 absorbed per unit of bed volume up to the time when the effluent CO_2 concentration reached 80 percent of feed.

The curve shape column specifies the general shape of the experimental breakthrough curve. The letters correspond to the general curve shapes shown in Figure 2-8.

2.4.1 Magnesium Oxide Compound Results (Table 2-4)

The first compound tested, M1, is the best compound developed during MDAC's early program to formulate a regenerable CO_2 scrubber for SCUBA. Tests with pure MgO pellets showed very low affimity for CO_2 and, thus, were not retested in this program. The wet version of M1 showed a capacity of 17.7 percent and provide a goal for additional development work. However, its physical strength is not adequate for repeated use. Thus, the screening of MgO compounds concentrated on finding a binder which will provide strength without sacrificing absorption capacity.

Sample M2 showed the addition of sodium silicate did not hinder the CO_2 capacity while showing some improvement in strength. Sample M3 shows that too much sodium silicate does hinder the sorption process, but a very strong pellet resulted. The use of asbestos as a binder in M4 resulted in a very

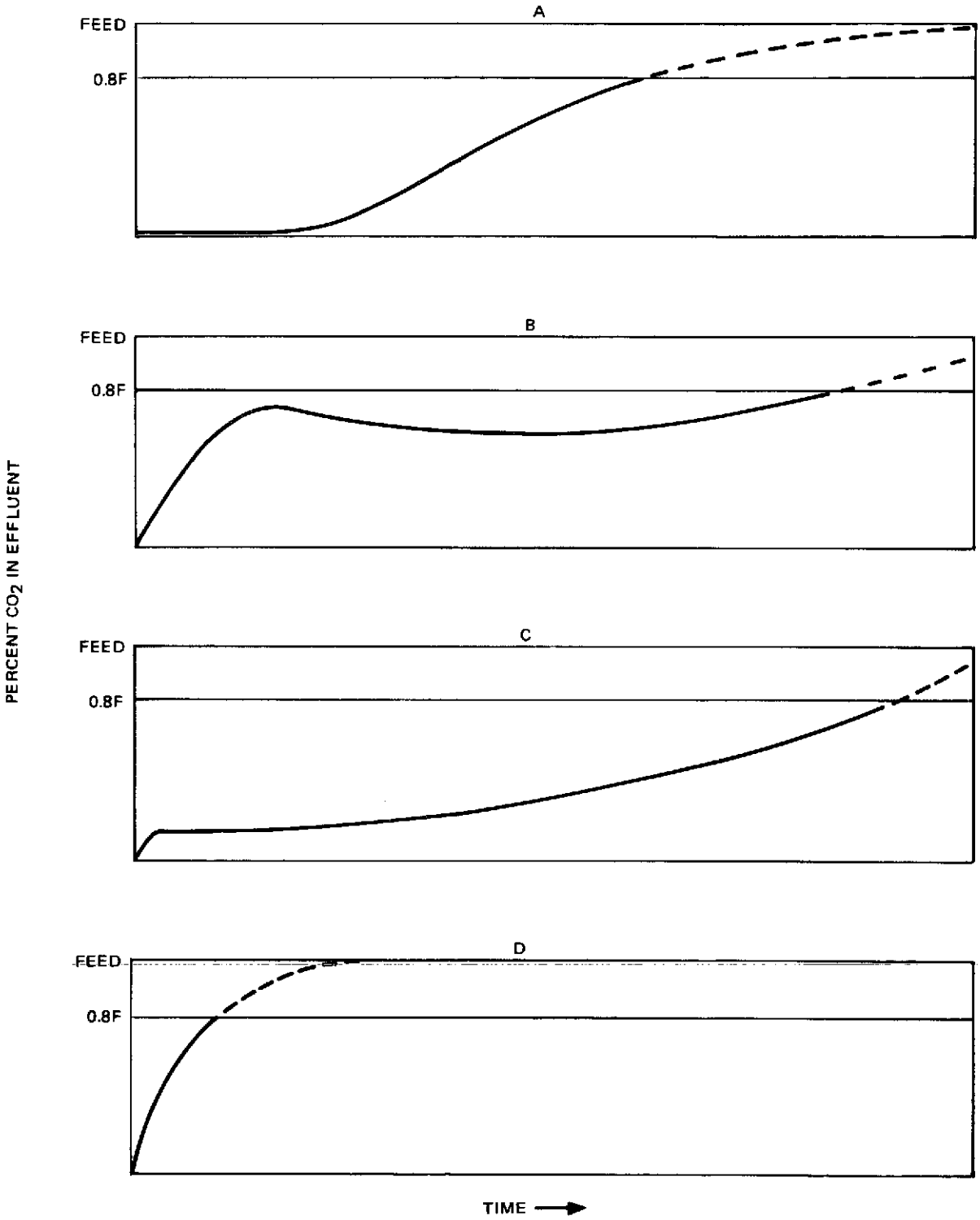

Figure 2-8. Typical Breakthrough Curve Shapes

Table 2-4

SCREENING RESULTS FOR MAGNESIUM OXIDE COMPOUNDS
(200 μm^3/min (cc/min) 1.1% CO_2 in N_2)

Sample No.	Composition	Bed Wt (mKg)	Time to BT (min)	Time to 80% Feed (hr)	Wt % CO_2 at BT	Wt % CO_2 at 80%	Bed Depth (m)	ρCO_2 mKg/μm^3 x 100	Curve Shape (Fig. 2-8)
M1D	86.2% MgO, 13.8% KOH	14.6	105	3.67	2.9	4.6	0.1	1.4	A
M1W	68.8% MgO, 11.0% KOH, 20.2% H_2O	21.2	210	19	4.0	17.7	0.1	7.6	A
M2D	83.8% MgO, 16.2% Na_2SiO_3	12.3	50	6	1.6	5.9	0.1	1.5	A
M2D2	83.8% MgO, 16.2% Na_1SiO_3	14.2	40	4	0.9	3.2	0.1	0.9	A
M3D	72.3% MgO, 27.7% Na_2SiO_3	14.8	20	3.75	-	2.8	0.1	0.8	A
M3W	56.4% MgO, 21.8% Na_2SiO_3, 21.8% H_2O	17.9	0	10	0	3.9	0.1	1.4	D
M4D	77.3% MgO, 14.3% KOH, 8.4% Asbestos	19.7	300	13.5	6.2	10.5	0.2	2.1	A
M5D	58.0% MgO, 31.0% Na_2SiO_3, 11.0% Asbestos	17.2	75	8	1.7	5.7	0.1	2.0	A
M5W	40.4% MgO, 21.6% Na_4SiO_3, 7.8% Asbestos, 30.2% H_2O	21.8	60	13	1.1	7.9	0.1	3.4	A
M6D	56.3% MgO, 10.7% KOH, 22.3% Na_2SiO_3, 10.7% Asbestos	13.2	15	7.5	-	6.4	0.1	1.7	B
M6W	32.5% MgO, 6.2% KOH, 12.9% Na_2SiO_3, 6.1% Asbestos, 42.3% H_2O	26.0	225	16.5	3.5	11.1	0.1	5.8	A
M6DW	36.1% MgO, 4.0% KOH, 14.3% Na_2SiO_3, 3.9% Asbestos, 35.7% H_2O	23.0	120	14	2.1	12.8	0.1	5.9	A
M6W2	32.7% MgO, 6.3% KOH, 12.9% Na_2SiO_3, 6.2% Asbestos, 41.9% H_2O	24.6	150	13.5	2.6	9.2	0.1	4.6	A
M6DW2	35.4% MgO, 6.8% KOH, 14.0% Na_2SiO_3, 6.7% Asbestos, 37.1% H_2O	21.3	80	14.5	1.5	10.5	0.1	4.5	A
M6DW3	41.6% MgO, 16.4% Na_2SiO_3, 7.8% Asbestos, 7.8% KOH, 26.2% H_2O	23.3	10	13.5	—	8.5	0.1	4.0	A
M6DW4	34.3% MgO, 13.6% Na_2SiO_3, 6.5% Asbestos, 6.5% KOH, 39.1% H_2O	23.5	10	12	—	9.8	0.89	5.3	A
M6DW5	40.1% MgO, 15.9% Na_2SiO_3, 7.6% Asbestos, 7.6% KOH, 28.8% H_2O	20.1	50	14	1.0	9.5	0.89	4.4	A
M8D	55.1% MgO, 15.6% KOH, 21.5% Na_2SiO_3, 7.8% Asbestos	15.1	5	7.5	-	5.6	0.1	1.7	B
M8W	32.8% MgO, 9.3% KOH, 12.8% Na_2SiO_3, 4.6% Asbestos, 40.5% H_2O	21.5	210	14.5	3.9	12.3	0.1	5.3	A
M8W2	31.1% MgO, 8.8% KOH, 12.2% Na_2SiO_3, 1.4% Asbestos, 43.5% H_2O	23.0	45	15	0.8	9.5	0.1	4.4	A
M9D	53.3% MgO, 19.7% Na_2SiO_3, 8.4% Asbestos, 18.6% K_2CO_3	12.5	100	10.0	3.2	9.3	0.1	2.3	A
M9D2	53.3% MgO, 19.7% Na_2SiO_3, 8.4% Asbestos, 18.6% K_2CO_3	13.7	30	6.5	0.9	5.5	0.1	1.5	B
M9D2W	30.4% MgO, 11.2% Na_2SiO_3, 4.8% Asbestos, 10.6% K_2CO_3, 43.0% H_2O	21.9	210	15.0	3.9	12.2	0.1	5.4	A
M9D2W2	28.4% MgO, 10.5% Na_2SiO_3, 4.5% Asbestos, 9.9% K_2CO_3m 46.7% H_2O	22.5	120	13.3	2.3	10.9	0.89	5.6	A
M10D	79.7% MgO, 20.3% LiI	10.0	160	12.5	6.8	17.1	0.11	3.1	A
M10D2	79.7% MgO, 20.3% LiI	10.1	75	6.0	3.4	8.3	0.1	1.7	A
M10W	49.1% MgO, 12.6% LiI, 38.3% H_2O	16.2	80	5.0	2.1	4.3	0.1	1.4	A
M11D	60.7% MgO, 15.5% LiI, 23.8% Na_2SiO_3	7.2	50	7.5	3.0	12.9	0.1	1.9	A
M12D	66.3% MgO, 17.0% LiI, 16.7% KOH	15.5	30	5.5	0.8	5.0	0.91	1.8	A
M12W	38.1% MgO, 9.8% LiI, 9.6% KOH, 42.5% H_2O	28.8	240	15	3.5	9.8	0.1	5.7	A
M12W2	42.2% MgO, 10.8% LiI, 10.7% KOH, 36.3% H_2O	25.9	180	10.25	2.9	7.0	0.1	3.4	A
M12W3	43.2% MgO, 11.1% LiI, 10.8% KOH, 34.9% H_2O	26.1	180	10.75	2.9	7.2	0.11	3.4	A

light and fragile pellet, but an apparent improvement in porosity was promising. The combination of Na_2SiO_3, asbestos, and KOH in samples M5 through M8 resulted in quite strong pellets with moderately good CO_2 capacities and apparently good regenerability.

The effect of the addition of moisture is quite evident when comparing all D versus W capacities. It should also be noted that most of the deviations from the desirable A-shaped breakthrough curve were dry tests.

2.4.2 Zinc Oxide Compound Results (Table 2-5)

The initial tests with zinc oxides Z1 and Z2 showed very promising results even in the dry condition. However, these pellets were very fragile and not suitable for repeated handling. These pellets were manufactured from $ZnCO_3$ – prepared by precipitation from mixing Na_2CO_3 and $ZnNO_3$ – due to unavailability of commercial $ZnCO_3$ during the early weeks of the program.

Subsequent tests with pellets made from AR-grade $ZnCO_3$, showed very poor activity as evidenced by the data for Z3 through Z10. Samples Z3, Z7, and Z8, which contained appreciable amounts of asbestos, plugged the pellet maker and could not be manufactured or tested.

After experiencing repeated poor results with the commercial $ZnCO_3$, it was suspected that Na^+ was being co-precipitated with the Zn^{++} in the material used in Z1 and Z2. A sample of the precipitated $ZnCO_3$ was dissolved in HCl and subjected to analysis by atomic absorption. The sample was found to contain 12.5 percent by weight Na which, assuming comparable activity to KOH with MgO, possibly explains the high activity of Z1 and Z2. Further analysis failed to show appreciable $NO_3^=$ in the sample, thus demonstrating that occluded Na_2CO_3 could be acting as a catalyst in Z1 and Z2.

Samples Z6 and Z10 with appreciable concentrations of Na_2SiO_3 show good strength but poor CO_2 capacities.

The co-precipitation phenomenon mentioned previously was investigated with samples Z11, Z12, and Z13. The co-precipitated Na did not appear to have much value as a catalyst. Sample Z14 shows relatively good capacity but

Table 2-5
ZINC COMPOUND SCREENING RESULTS
(200 μm^3/min (cc/min) 1.1% CO_2 in N_2)

Sample No.	Composition	Bed Wt (mKg)	Time to BT (min)	Time to 80% Feed (hr)	Wt % CO_2 at BT	Wt % CO_2 at 80%	Bed Depth (m)	pCO_2 mKg/μm^3 x 100	Curve Shape (Fig. 2-8)
Z1D	100% ZnO	16.2	15	18	–	17.2	0.1	5.6	C
Z1W	87.8% ZnO, 12.2% H_2O	18.8	10	22	–	15.0	0.1	5.0	C
Z2D	88.1% ZnO, 11.9% KOH	31.4	375	21	4.0	10.5	0.18	3.8	A
Z2D2	88.1% ZnO, 11.9% KOH	28.6	70	34.5	1.0	17.9	0.15	6.9	A
Z3	71.9% ZnO, 16.5% Na_2SiO_3, 11.6% Asbestos	–	–	–	–	–	–	–	–
Z4D	100% ZnO	13	10	4.5	–	3.2	0.1	0.8	B
Z5D	86% ZnO, 14% Na_2SiO_3	15	0	1/2	–	–	0.13	–	D
Z6D	74.9% ZnO, 11.9% KOH, 13.2% Na_2SiO_3	18.6	10	10.75	–	4.4	0.1	1.6	B
Z6W	59.4% ZnO, 9.5% KOH, 10.5% Na_2SiO_3, 20.6% H_2O	25.3	0	450	–	2.1	0.11	1.0	B
Z7	69.9% ZnO, 11.3% KOH, 18.8% asbestos	–	–	–	–	–	–	–	–
Z8	77.1% ZnO, 10.4% KOH, 12.9% asbestos	–	–	–	–	–	–	–	–
Z9D	92.0% ZnO, 5.0% KOH, 3.0% asbestos	14.3	5	2	–	–	0.1	–	B
Z10D	69.1% ZnO, 10.2% KOH, 20.7% Na_2SiO_3	21.5	0	7	0	2.2	0.1	0.9	B
Z10W	50.1% ZnO, 7.4% KOH, 15.0% Na_2SiO_3, 27.5% H_2O	30.9	0	1.25	–	–	0.1	–	D
Z11D	100% ZnO	15.6	5	5.8	–	3.5	0.1	1.1	B
Z11W	51.2% ZnO, 48.8% H_2O	30.5	0	12.5	–	4.0	0.08	2.8	B
Z12D	100% ZnO (contains 6.9% Na)	19.7	0	15.5	–	12.5	0.1	5.0	C
Z13D	13.4% ZnO, 26.6% $NaSiO_3$	21.2	0	11.5	–	6.2	0.1	2.6	B
Z13DW	48.1% ZnO, 17.5% $NaSiO_3$, 34.4% H_2O	24.6	0	12.0	–	4.8	0.08	2.7	B
Z14D	60.7% ZnO, 11.7% HzOH, 27.6% Na_2SiO_3	21.4	30	36	0.56	15.5	0.1	6.7	B
Z14D2	60.7% ZnO, 11.7% NaOH, 27.6 Na_2SiO_3	26.2	0	28.5	–	15.3	0.1	8.1	B
Z14D3	60.7% ZnO, 11.7% NaOH, 27.6% Na_2SiO_3	26.1	0	29.5	–	14.9	0.1	7.8	B
Z14D3W	37.3% ZnO, 7.2% NaOH, 17.0% Na_2SiO_3, 38.5% H_2O	42.9	0	21.5	–	7.9	0.1	6.8	C
Z14D3W2	49.4% ZnO, 9.5% NaOH, 22.4% Na_2SiO_3, 18.7% H_2O	32.5	60	20.0	0.8	9.1	0.1	5.9	C
Z15D	66.8% ZnO, 16.6% Clay, 16.6% KOH	28.1	35	2.3	0.5	1.7	0.05	1.4	A
Z16D	81.8% ZnO, 18.2% $AgNO_3$	38.5	0	0	0	0	0.07	0	D
Z17D	72.2% ZnO, 27.8% Zn Cl_2	22.3	0	0	0	0	0.1	0	D
Z18D	66.4% ZnO, 33.6% KH_2 PO_4	17.8	0	0	0	0	0.1	0	D

the rate is poor and the pellets are extremely fragile. The only hard pellet is Z15 but it is useless as a CO_2 sorber. The tests with some of the new binder candidates appear as Z16, Z17, and Z18. In general, the structures showed promise but no CO_2 affinity is evident.

2.4.3 Silver Compound Results (Table 2-6)

The early samples of silver oxide pellets show essentially the same behavior as the magnesium oxide compounds. In general, all samples showed very low sorption rates except S2DW, which was the only sample with an A-shaped curve. The use of KOH as a catalyst appears to be beneficial in improving the capacity as well as the sorption rate of silver oxide.

The addition of sodium silicate in S3 resulted in quite strong pellets. The capacity of S3 is quite good both wet and dry; however, during the dry test the CO_2 concentration of the effluent was greater than 0.65 percent during the entire test.

The early results with silver oxide using potassium hydroxide and sodium silicate individually as additives showed both give rather good total capacities and promising structural properties but poor sorption rates. Compound S4 includes both additives (see Table 2-7 for composition) and excellent results were obtained. Table 2-7 lists data from 28 regenerations. This material has shown no tendency to degrade in activity with the exception of run number 23 where there was reason to believe that the regeneration was not conducted properly. In all cases, regeneration was carried out by removing the pellets from the tube, placing them in an evaporating dish, and heating in a preheated oven at 523°K for two hours. The regenerated pellets have a very dark brown color, while the expended material has a greenish tint.

The sorption rate showed a marked improvement during the first few regenerations. This was probably due to some structural changes occurring, since after the fifth regeneration some degradation in pellet hardness was noted. This process apparently continues since the bed volume is increased in spite of loss of material due to spillage. Some dusting during handling became apparent sometime after 10th regeneration.

Table 2-6
SILVER COMPOUND SCREENING RESULTS
(200 μm^3/min (cc/min) 1.1% CO_2 in N_2)

	% Oxide	% KOH	% Na_2SiO_3	% KCNS	% Y_2O_3	% H_2O	Bed Wt (mKg)	Time to BT (min)	Time to 80% Feed (hr)	Wt % CO_2 at BT	Wt % CO_2 at 80% Feed	Bed Depth (m)	pCO_2 mKg/μm^2 x 100	Curve Shape (Fig. 2-8)
S1D	100	-	-	-	-	-	38.0	0	14	0	5.4	0.07	5.6	C
S1DW	97.0	-	-	-	-	3.0	36.5	0	13.5	0	5.6	0.09	5.6	C
S2D	88.5	11.5	-	-	-	-	38.7	0	21.5	0	7.6	0.09	6.7	C
S2DW	79.5	10.4	-	-	-	10.1	41.3	330	21.5	3.2	9.4	0.09	8.9	A
S3D	90.1	-	9.9	-	-	-	57.4	0	57	0	9.8	0.09	12.9	B
S3DW	73.3	-	8.1	-	-	17.6	64.7	0	33	0	8.5	0.09	12.6	C
S4D	See Table 2-7													
S5D	77.5	-	-	22.5	-	-	57.4	0	0	0	0	0.12	0	D
S6D	98.8	-	-	-	1.2	-	49.3	0	22	0	3.1	0.11	4.8	C
S6D2	98.8	-	-	-	1.2	-	49.3	0	40	0	9.4	0.1	8.9	C
S6D3	98.8	-	-	-	1.2	-	49.4	0	40	0	12.5	0.091	12.6	C
S7D	See Table 2-8													

Table 2-7
BREAKTHROUGH DATA FOR COMPOUND S4
(Composition 80.3% Ag_2O, 10.4% KOH, 9.3% Na_2SiO_3)

Regeneration Number	Bed Wt (mKg)	Bed Depth (m)	Flow (μm^3/min)	Time to BT (min)	Time to 80% Feed (hr)	Weight % CO_2 at BT	Weight % CO_2 at 80%	ρCO_2 $mKg/\mu m^3$ x 100	Curve Shape (Fig. 2-8)
1	64.9	0.1	200	45	50.0	0.3	15.0	19.5	A
2	64.8	0.1	200	720	39.5	4.5	13.8	18.0	A
3	64.0	0.1	200	960	44.0	6.0	15.2	19.5	A
4	63.9	0.1	200	1080	36.3	9.8	13.5	17.2	A
5	62.7	0.1	200	1200	43.0	7.8	15.5	19.5	A
6	58.5*	0.1	200	1140	38.5	8.2	16.5	19.4	A
7	58.1	0.1	200	1260	38.0	8.8	15.5	18.1	A
8	58.6	0.1	200+	1680	47.0	9.9	17.1	20.1	A
9	58.9	0.1	200	1440	45.0	8.4	15.9	18.8	A
10	59.3	0.1	200	1620	47.0	9.4	16.5	19.6	A
11	58.4	0.1	200	1260	42.5	8.7	15.8	18.5	A
12	57.5*	0.1	200	1320	41.5	9.2	15.6	18.0	A
13	57.6	0.1	200	840	44.0	5.9	15.6	18.0	A
14	57.3	0.11	200	1260	40.5	8.9	14.6	15.0	A
15	57.3	0.12	1100	15	12.0	--	14.5	13.3	C
16	57.9	0.12	1050	10	12.0	--	13.4	12.5	C
17	57.2	0.12	1030	15	12.3	--	14.8	13.6	C
18	57.3	0.12	1500	10	9.5	--	14.3	13.2	B
19	57.3	0.13	1400	10	9.8	--	14.0	11.4	B
20	56.9	0.13	1980	0	8.3	--	14.6	11.8	B
21	57.0	0.13	1900	0	8.2	--	13.5	11.0	B
22	58.0	0.14	200	1080	40.8	7.9	15.8	12.7	A
23	58.6	0.15	200	240	34.0	1.7	12.5	10.2	A
24	56.0++	0.15	200	1320	40.5	10.0	17.1	12.8	A
25	55.7	0.15	200	1020	41.0	7.8	16.0	12.2	A
26	55.7	0.15	200	1080	43.0	8.3	15.9	12.2	A
27	53.3++	0.16	200	980	36.0	7.8	14.8	10.1	A
28	53.3	0.16	200	1020	36.0	8.2	15.2	11.1	A

* Pellets spilled, some lost

\+ Feed gas composition found to be erroneous, previous data questionable ±10%

++Fines removed

Runs 15 through 21 were conducted at increasing flow rates in an effort to get some idea of the sorption rate under conditions expected in an AEPS. Breakthrough curves for these runs are shown in Figure 2-9.

Some indication of rate-controlling mechanisms may be deduced from these data. At any point in time, doubling the flow rate does not double the effluent concentration. Thus, the major factor in controlling the CO_2 sorption rate is probably mass transfer at the surface of the pellet.

Sample S5 was the result of the binder development studies described in Section 2.4.5. It showed no affinity for CO_2.

Sample S6 was manufactured by the method described by Culbertson in Reference 5. He found the presence of 1 percent Y^{+++} ion to greatly enhance the performance of silver oxide. The data for S6 in Table 2-6 show quite good CO_2 capacities, which increased with each regeneration. However, the rate was very poor as evidenced by immediate breakthroughs.

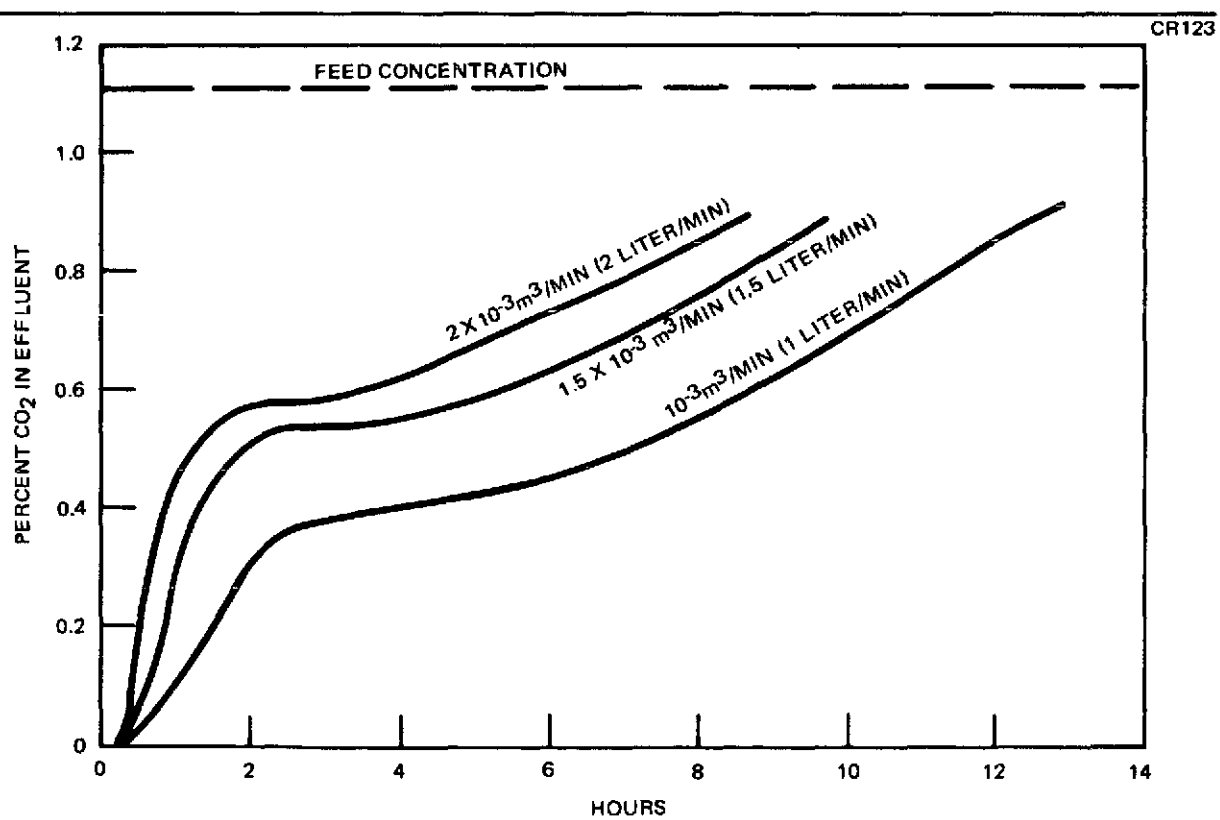

Figure 2-9. Breakthrough Curves for Compound S4 (Simulated Worst Case AEPS Atmosphere)

Sample S7 was manufactured with exactly the same composition as S4 to provide verification of S4's attractive behavior and a source of specimens for detailed analyses. Table 2-8 lists the breakthrough results for the 22 regenerations of S7. The regeneration process was modified somewhat in that the pellets were retained in the sorption tube during regeneration. In addition, the tube was placed in a cold furnace and allowed to heat up with the furnace. This change in procedure is assumed to be the cause of extremely stable pellet structure through 22 regenerations. No dusting or crumbling was observed, in contrast with S4 which began to dust after 12 regenerations. Several runs were made at high flow rates verifying the curves for S4 in Figure 2-9. Some of these are shown in Figures 2-10, 11, and 12. In addition, water breakthrough curves are shown. If one looks closely at the point where the CO_2 breakthrough occurs, it appears to correspond to the second knee in all three water curves. It has been postulated that the potassium present in this composition is present as K_2CO_3. If the K_2CO_3 reacts with H_2O and CO_2 forming $KHCO_3$, it may explain the correlation between these curves since the exhaustion of K_2CO_3 would then lower both CO_2 and H_2O sorption rates.

Runs 20 and 21 were made with a CO_2 concentration of 399 N/m^2 (3 mm Hg). The resulting capacities, approximately 12 percent, show a potential use for this material for the control of CO_2 in space cabins in light of the newer low CO_2 partial pressure requirements. Breakthrough curves are shown in Figure 2-13.

Sample Number 12 was run with the humidifer maintained in an ice bath, thus resulting in a dew point in the feed stream of 273°K. The resulting poor performance clearly points out the importance of moisture in the sorption mechanism.

Figure 2-14 shows a compilation of the capacity data from Tables 2-7 and 2-8 for samples S4 and S7. No degradation in performance is evident (within the scatter of the data) through more than 20 regenerations. Some of the lower points were from the high flow runs which is understandable since the tests were terminated at 80 percent breakthrough.

Table 2-8

BREAKTHROUGH DATA FOR COMPOUND S7
(Same Composition as S4)

Sample No.	Bed Wt (mKg)	Bed Depth (m)	Flow μm^3/min	Time to BT (min)	Time to 80% Feed (hr)	Wt % CO_2 at BT	Wt % CO_2 at 80%	ρCO_2 mKg/μm^3 x 100	Curve Shape (Fig. 2-8)	Remarks
1	49.8	0.12	200	60	39.0	0.4	12.4	10.3	A	
2	49.8	0.12	200	1080	36.5	8.1	12.0	12.2	A	
3	49.8	0.12	200	1320	38.5	9.9	14.9	12.3	A	
4	46.5	0.115	200	1320	37.0	10.6	15.8	13.0	A	Sample taken
5	46.5	0.115	200	1260	36.1	10.2	16.2	13.4	A	
6	46.5	0.115	1000	20	10.5	0.8	15.8	13.0	A	
7	46.5	0.115	1000	20	9.2	0.8	14.6	12.1	A	
8	44.3	0.11	200	360	36.8	11.1	16.5	13.8	A	Sample taken
9	43.9	0.11	1500	0	7.2	0	14.4	11.7	A	Sample taken
10	43.9	0.11	1500	0	7.0	0	13.4	11.1	A	
11	43.9	0.11	1000	20	8.5	0.8	13.7	11.4	A	
12	43.9	0.11	1000	0	3.5	0	5.0	2.1	A	Dew point 273 °K
13	43.1	0.1	200	1500	38.5	11.4	16.2	14.6	A	Sample taken
14	43.1	0.1	1000	20	9.0	0.8	14.2	12.2	A	
15	43.1	0.1	200							Ran out of gas
16	43.1	0.1	600	75	12.8	0.6	14.6	12.6	A	
17	43.1	0.1	200	1320	39.2	10.7	16.3	14.6	A	
18	43.1	0.1							A	Flow rate unknown
19	43.1	0.1	600	60	13.0	0.4	13.9	12.0	A	
20	43.1	0.1	1000	0	22.0	0	13.0	11.2	A	Feed 0.39% CO_2
21	43.1	0.1	1500	0	19.0	0	14.5	12.5	A	Feed 0.39% CO_2
22	43.1	0.1	200	900	35.0	8.0	15.5	13.4	A	

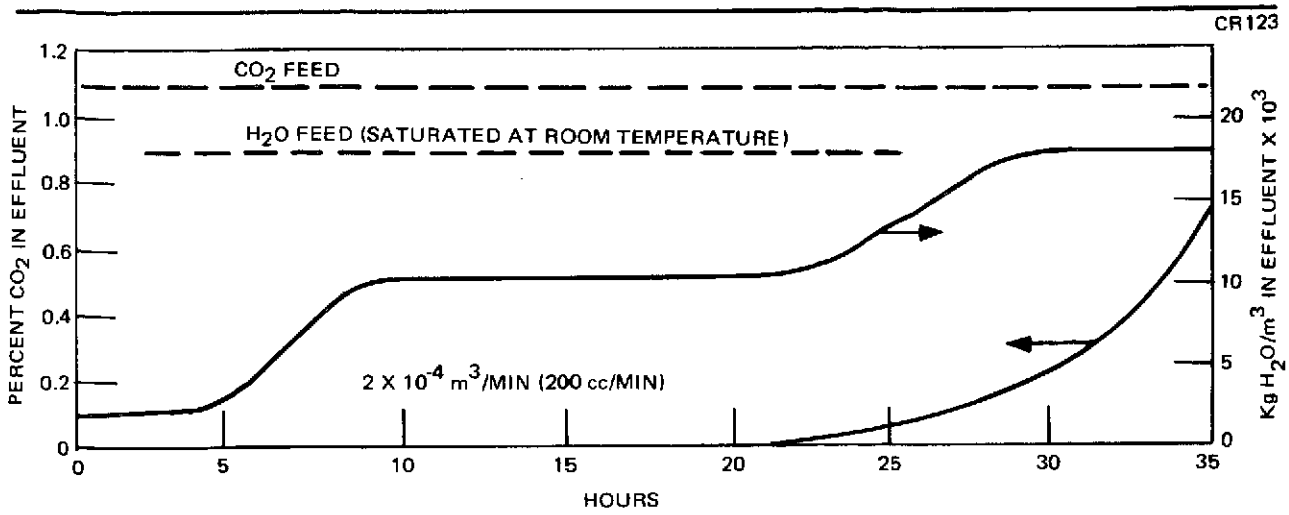

Figure 2-10. Run S7D5 Breakthrough Curves

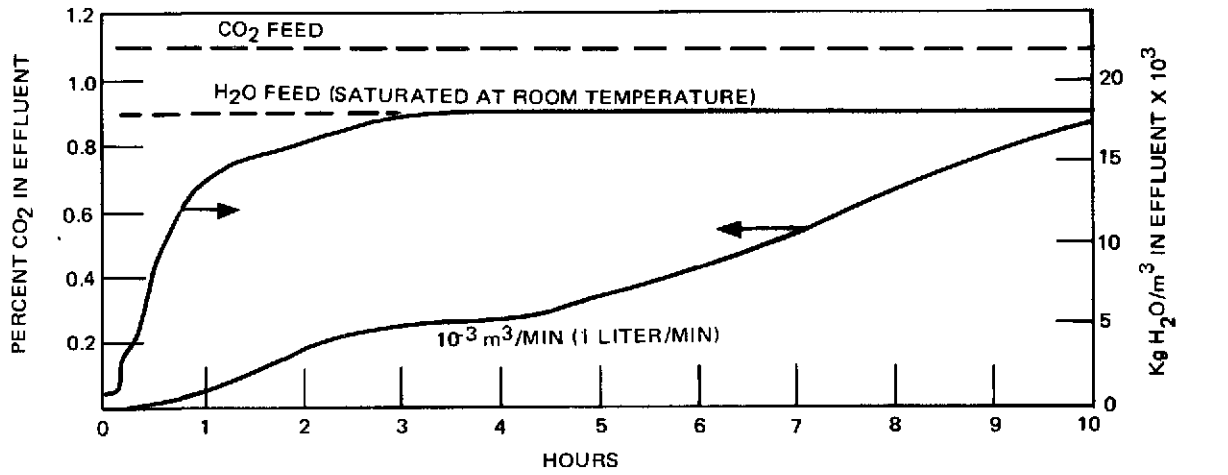

Figure 2-11. Run S7D6 Breakthrough Curves

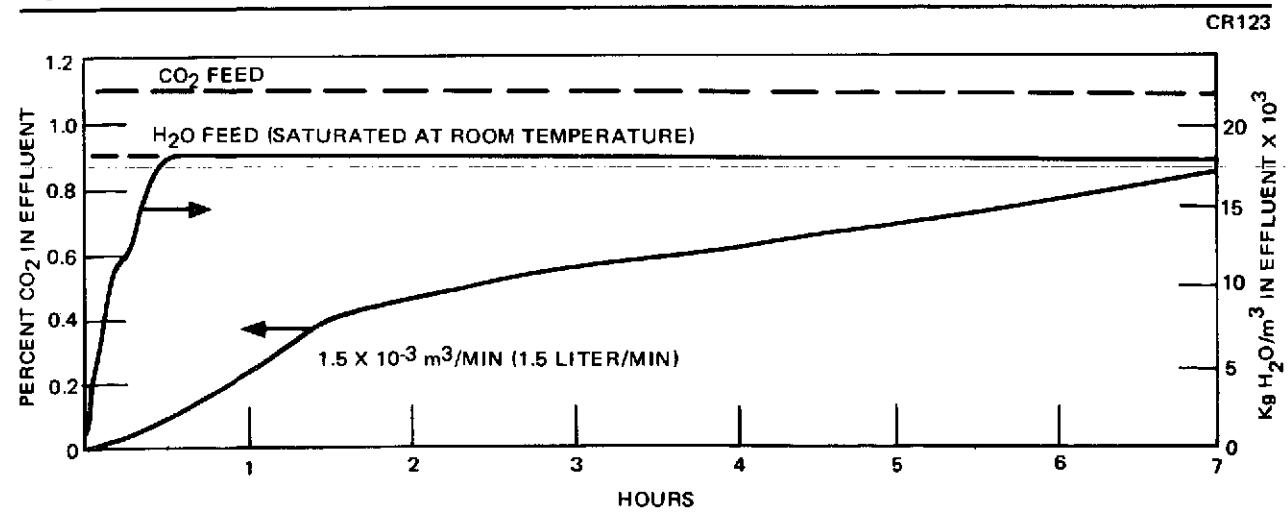

Figure 2-12. Run S7D10 Breakthrough Curves

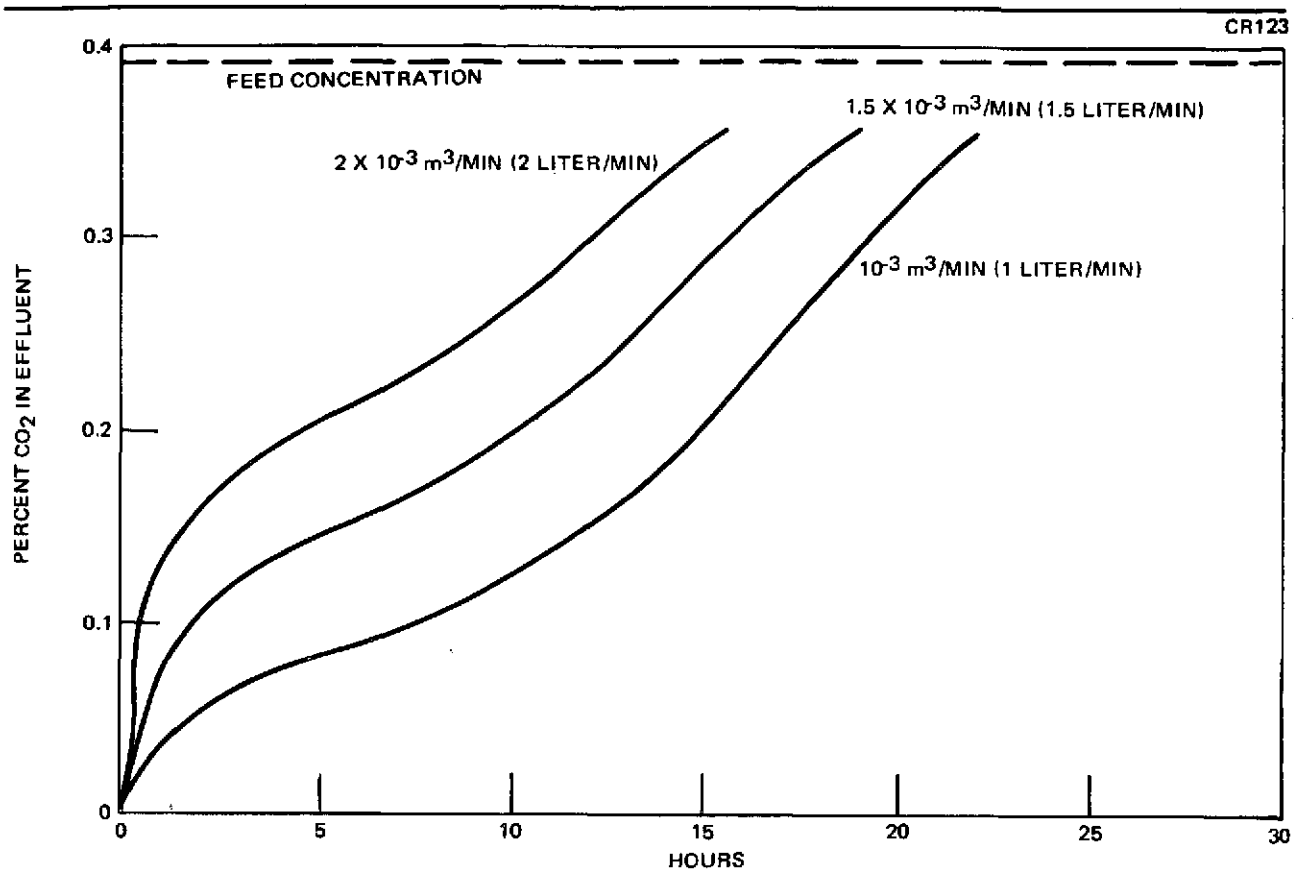

Figure 2-13. Breakthrough Curves for Compound S7 (Simulated Space Cabin Atmosphere)

2.4.4 Metallic Hydroxide Results

The results from tests on magnesium and zinc hydroxides are shown in Table 2-9.

Data for M13D and M14D on Table 2-9 show rather disappointing affinities for CO_2 by $Mg(OH)_2$. These results show that the mechanism previously assumed for the wet magnsium oxide formulations involving $Mg(OH)_2$ are probably in error. It appears that $Mg(OH)_2$ has very little affinity for CO_2.

The subsequent regenerations of M13 and M14 are reported as MgO compounds since $Mg(OH)_2$ decomposes at about $523^{\circ}K$ and $723^{\circ}K$ is used for regeneration.

Sample Z19D on Table 2-9 shows very poor affinity for CO_2. Regeneration resulted in ZnO with no observable reaction in spite of a very low density.

2.4.5 Pellet Binder Studies

Experience to date has shown that sodium silicate is useful as a binder for

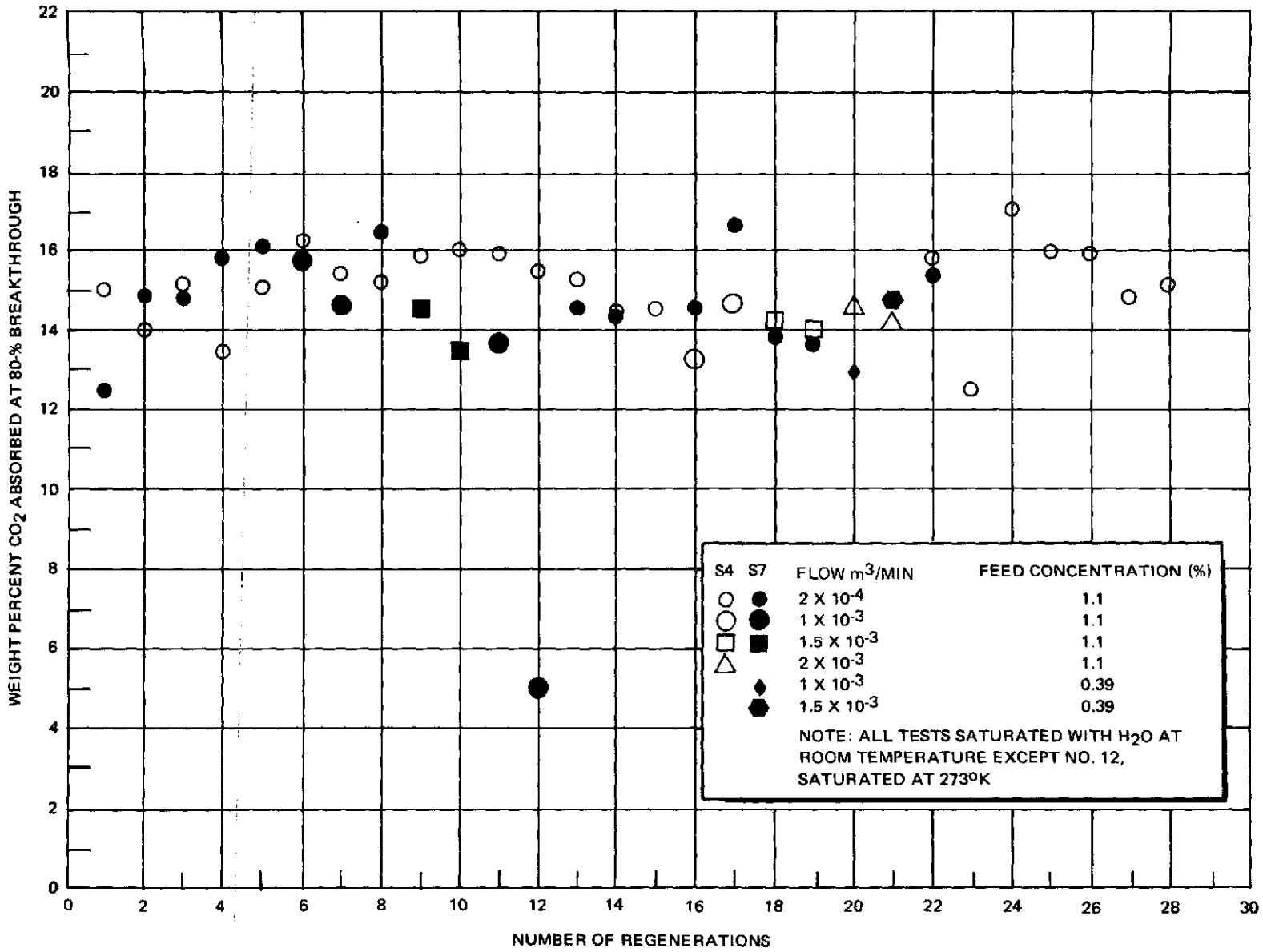

Figure 2-14. Regeneration Histories of Compounds S4 and S7

Table 2-9
SCREENING RESULTS FOR METALLIC HYDROXIDES
(200 μm^3/min (cc/min) 1.1% CO_2 in N_2)

Sample No.	Composition	Bed Wt (mKg)	Time to BT (min)	Time to 80% Feed (hr)	Wt % CO_2 at BT	Wt % CO_2 at 80%	Bed Depth (m)	ρCO_2 mKg/μm^3 x 100	Curve Shape (Fig. 2-8)
Z19D	$Zn(OH)_2$	24.0	0	14.5	0	4.0	0.1	1.9	B
Z19D2	ZnO	17.4	0	0	0	0	0.09	0	–
M13D	$Mg(OH)_2$	21.5	0	23.5	0	9.6	0.1	4.1	B
M13D2	MgO	16.5	0	11.0	0	5.2	0.82	2.1	B
M13D2W	57% MgO, 43% H_2O	27.0	0	7.35	0	2.4	0.12	1.1	B
M14D	90% $Mg(OH)_2$, 10% KOH	30.3	0	8.0	0	1.3	0.82	1.0	B
M14D2	86% MgO, 14% KOH	23.0	0	7.75	0	3.0	0.82	1.7	B
M14D2W	55.7% MgO, 9.1% KOH, 35.2% H_2O	35.2	0	8.5	0	1.4	0.89	1.1	B
M14D2W2	54.2% MgO, 8.8% KOH, 37.0% H_2O	32.7	0	8.0	0	1.9	0.89	1.4	B

magnesium and silver compounds but is only marginally effective with zinc. The gradual softening of the silver oxide pellets described for sample S4 was thought to be due to the repeated changing of the crystal structure from silver oxide to silver carbonate. A new approach to a binder concept which could completely restructure the pellet during each regeneration would be desirable. If a stable material can be found which melts and recrystallizes at slightly below the regeneration temperature, the above concept may be realized.

Table 2-10 lists some compounds which have been identified with attractive physical properties. Tests were made on most materials by preparing small samples and comparing the hardness after exposure to regeneration conditions. The results column of Table 2-10 shows that in most cases the binding effect was quite disappointing. The one material that showed promise was KCNS. However, pellets made from silver carbonate and KCNS had very good structural properties but showed absolutely no affinity for CO_2. Subsequent investigations showed that KCNS solutions give an acid reaction with pH indicators. This property, of course, explains the inability of materials containing KCNS to absorb CO_2. This property was also observed with many of the other potential binders, especially the salts of strong acids and weak bases such as $ZnCl_2$. The organic binders were also found to be ineffective. Invariably, they decomposed, when mixed with the metal carbonates and heated, well below their listed melting points. Both pyrogallol and erythritol reduced the Ag_2O to metallic silver, but produced a very strong sponge-like structure which may be valuable as a method of manufacturing high surface area silver electrodes, etc.

The clay binder used in the manufacture of molecular sieves was investigated. When mixed with the carbonates of zinc and magnesium, a strong structure could not be obtained. The clay when mixed with ZnO and fired at 1,473°K yielded a very strong and hard pellet. However, it showed no affinity for CO_2.

2.4.6 Crush Strength Test Results

The crush strengths of the majority of pellets manufactured were measured, using the apparatus shown in Figure 2-7, as described in Section 2.3.3. The

Table 2-10
CANDIDATE FUSION BINDER COMPOUNDS

Compound	Melting Point (°K)	Boiling Point (°K)	Solubility mKg/100 μm^3 H_2O	Results Ag	Zn
$SnCl_2$	520	896	84	Acid	Acid
$AgNO_3$	485	717	122	Poor	Good with ZnO
KCNS	545	773	177	Very good	Good with ZnO
$FeCl_3 \cdot 6H_2O$	310	533	246	Poor	Poor
$ZnCl_2$	535	1,005	432	Acid	Acid
$Mg(NO_3)_2 \cdot 6H_2O$	368	603	42	Promising	Poor
$CuSO_4$	473	923	32	Acid	Acid
Antipyrene	383	592	100	Poor	Poor
Diethylamine Hydrochloride	503	593	252	NT	NT
Pyrogallol	407	582	62	Reduces to Ag	Poor
Erythritol	399	603	60	Reduces to Ag	Poor
4 Pyridol	421	623	100	NT	NT
				Mg	
CuCl	695	1,639	1.5	Acid	
LiI	719	1,463	151	Basic, promising	
$SnCl_2$	520	896	84	Poor, acid	

NT — Not tested to date

results of these tests are shown in Table 2-11. Some of the magnesium compounds containing Na_2SiO_3 show strength comparable to or exceeding molecular sieve and silica gel. The only zinc compounds which showed any strength were these manufactured as a result of the binder studies, Z15, Z16, and Z18. None of these showed any affinity for CO_2 due to the acidic characteristics of the binders. Sodium silicate did not work at all with ZnO even at concentrations as high as 27 percent in Z13.

The strength of the silver compounds containing Na_2SiO_3 was quite good. Sample S3 was the first attempt using Na_2SiO_3 and sample S4 held its strength through five regenerations; however, thermal shocking apparently degraded the pellets, as evidenced by S4D28. The degradation appears to be greatly attenuated by the slower regeneration process as used in S7. However, some degradation is evident. Further modifications of the regeneration process may reduce this even more.

2.4.7 Regeneration Studies

The regeneration characteristics of compounds S4 and S7 were studied using the apparatus shown in Figure 2-6 as described in Section 2.3.2. The first regeneration of S4 was carried out by increasing the oven temperature step-wise and watching the CO_2 evolution rate. The results of this test are shown in Figure 2-15. Up to 425°K, each increase in temperature caused an increase in CO_2 evolution which then slowely decreased again. At 425°K, the CO_2 rate remained constant over 1.5 hours and the next two temperature increases caused increasing but stable evolution rates. It is postulated that in the early phase, adsorbed CO_2 was evolved with each temperature increase since the relative quantities were quite small. During the stable periods, it is assumed that the $Ag_2CO_3 \rightleftharpoons AgO + CO_2$ equilibrium is maintaining the appropriate partial pressure for that temperature. If one looks at Figure 2-1 and determines the equilibrium CO_2 partial pressure for the region between 400 and 500°K, one may calculate the pressure to be between 10^3 and 10^5 N/m^2 (or 10^{-2} to 1 atm or 1 to 100 percent). Since the N_2 feet rate was 100 μm^3/min (100 cc/min), the concentration in this region calculates to be between 0 and 20 percent. When the temperature reached 500°K, the amount of residual Ag_2CO_3 was probably depleted, thus equilibrium could not be maintained.

Table 2-11
PELLET CRUSH STRENGTH

Magnesium Compounds	Crush Strength N	Crush Strength lb
M1	8.9	2.0
MA1	4.4	1.0
M2	13.8	3.1
M3	35.6	8.0
M4	13.8	3.1
M5	36.5	8.2
M6	17.8	4.0
M7	17.8	4.0
M8	13.4	3.0
M9	13.8	3.1
M10	4.4	1.0
M11	4.4	1.0
M12	8.9	2.0

Zinc Compounds	Crush Strength N	Crush Strength lb
Z1	13.4	3.0
Z2	11.1	2.5
Z4	3.6	0.8
Z5	3.1	0.7
Z6	4.0	0.9
Z9	3.6	0.8
Z10	4.4	1.0
Z11	3.6	0.8
Z13	6.6	1.5
Z14	8.9	2.0
Z15	44.9	10.1
Z16	36.1	8.1
Z17	5.3	1.2
Z18	44.5	10.0
Z20	9.8	2.2

Silver Compounds	Crush Strength N	Crush Strength lb
S1	4.4	1.0
S2	5.3	1.2
S3	24.5	5.5
S4D5	27.1	6.1
S4D28	3.6	0.8
S5	4.1	9.2
S6	4.4	1.0
S7D1	16.9	3.8
S7D4	32.0	7.2
S7D8	13.4	3.0
S7D12	12.5	2.8
S7D19	9.8	2.2

Other Compounds	Crush Strength N	Crush Strength lb
Molecular Sieve	21.2	5.0
Silica Gel	31.1	7.0

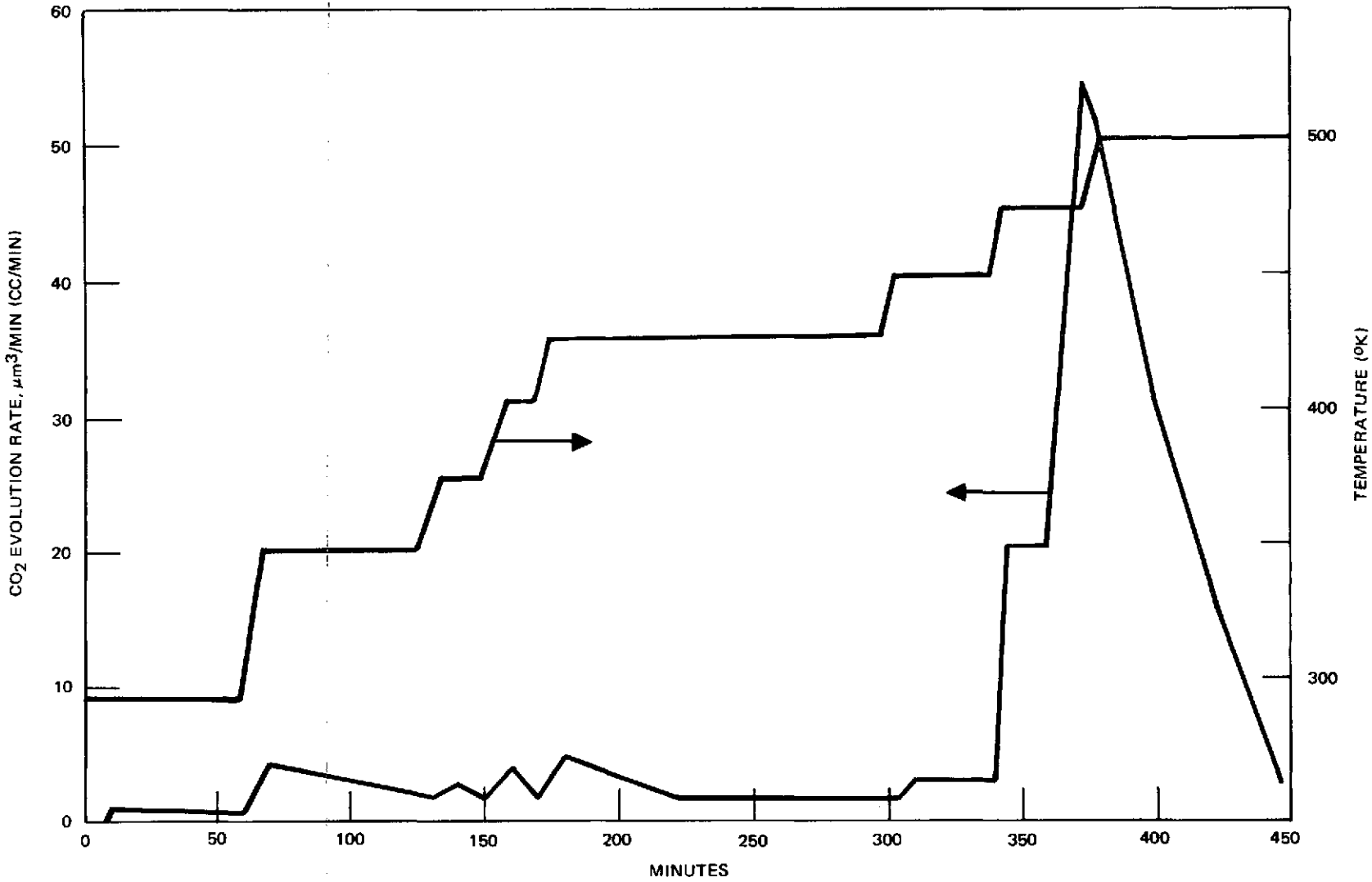

Figure 2-15. Stepwise Regeneration of Compound S4

Figure 2-16 shows a regeneration of sample S7D4 with the oven control set at its lowest power setting. Approximately 40 minutes were required for the oven to reach 500°K. An early low temperature spike is evident followed by the majority of CO_2 evolving when the bed temperature went past 450°K. An extremely slow trailoff was encountered until the temperature was increased to 525°K. The rate then went directly to zero.

During the test shown in Figure 2-17, the oven was heated to 525°K at the fastest rate possible, attaining the temperature in less than 10 minutes. The same general evolution curve shape was obtained; however, the time span was much shorter.

Figure 2-18 shows a regeneration in which a diaphragm pump was used to reduce the pressure in the bed to less than 1,100 N/m^2 (8 mm Hg). The evolution curve was smoothed, probably due to mixing in the added plumbing, but the regeneration time was greatly reduced again. This is the process that would be used to regenerate an AEPS cartridge when the CO_2 is to be fed directly to an oxygen recovery system.

The above procedure was carried one step further by using a Welch roughing pump and stopping the N_2 purge. This process was carried out on sample S7D16 for four hours at 525°K. The high capacity of S7D17 shows that this is a staisfactory method of regeneration. An evolution curve could not be made due to the exhaust characteristics of the pump.

2.5 DETAILED ANALYSIS OF SAMPLES

Some of the more promising samples were subjected to detailed chemical and physical analyses in an attempt to identify those properties which could be correlated to desirable sorption and physical characteristics.

2.5.1 Thermogravimetric Analysis (TGA)

This technique involves monitoring the weight loss of a small sample as a function of temperature in any desired atmosphere environment. The equipment also measures the instantaneous rate of change at a given point.

Figure 2-19 shows the decomposition characteristics of the three carbonates of interest. The rate of change of basic magnesium carbonate shows two

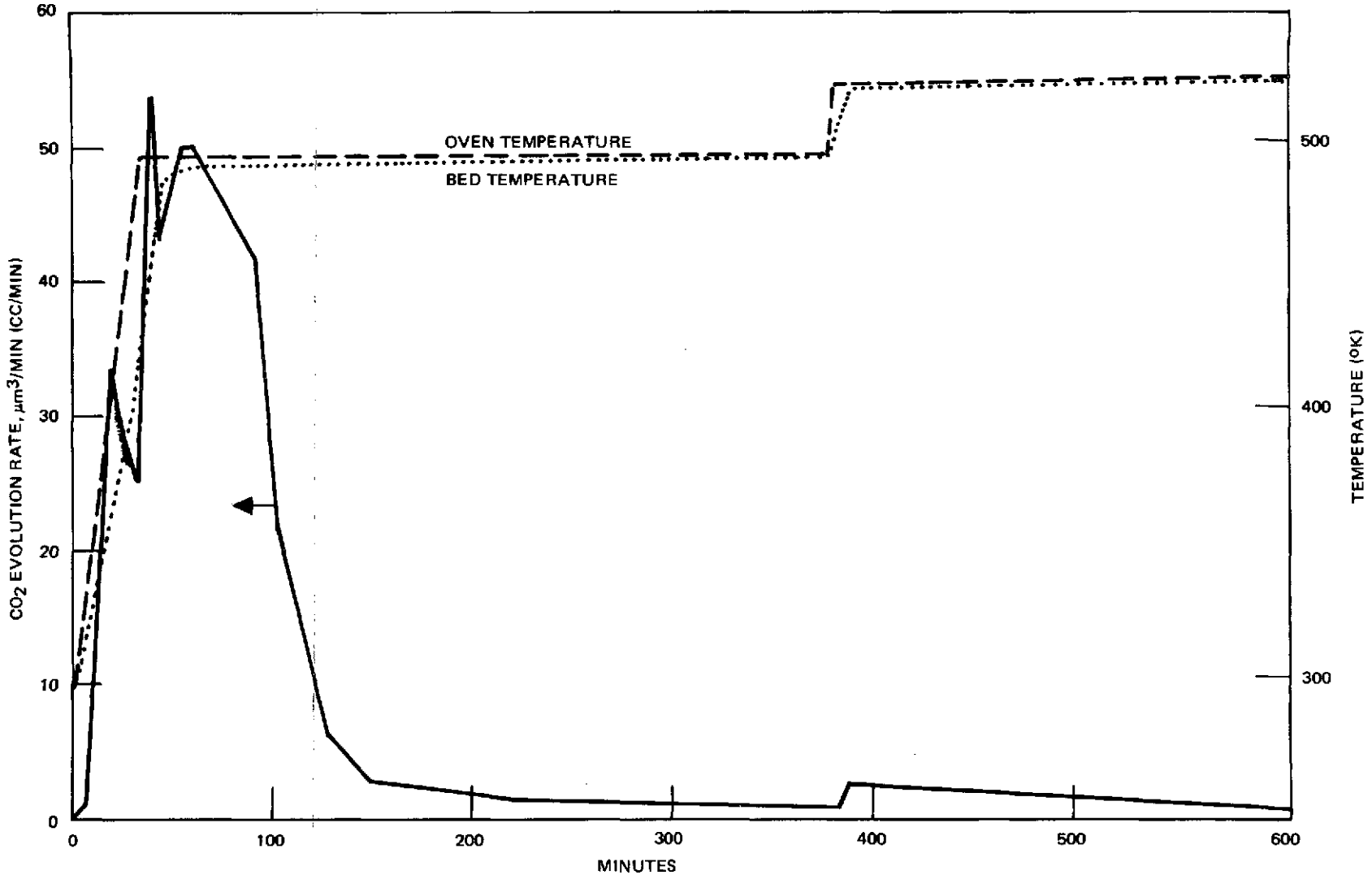

Figure 2-16. Regeneration of S7D4

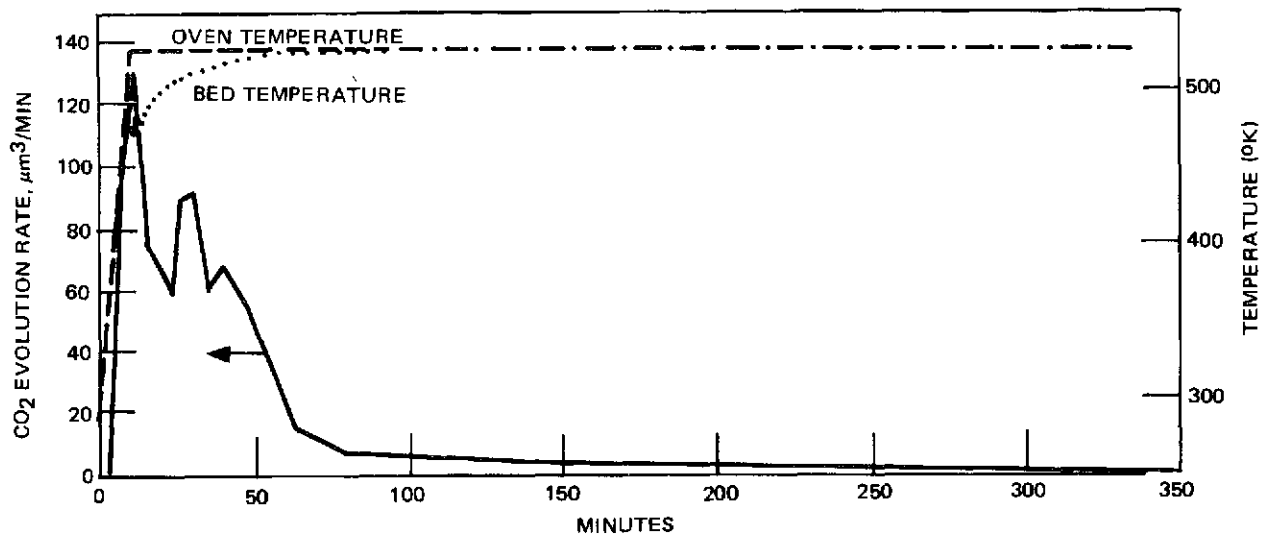

Figure 2-17. Regeneration of S7D5

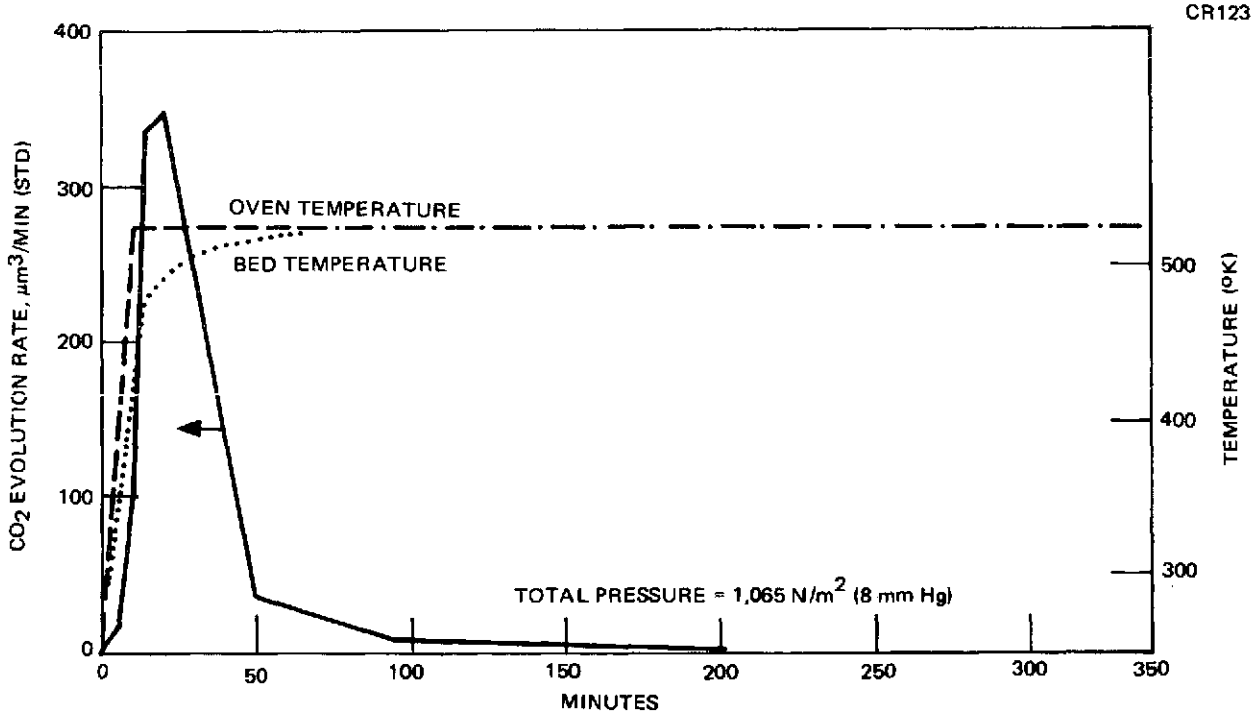

Figure 2-18. Regeneration of S7D10

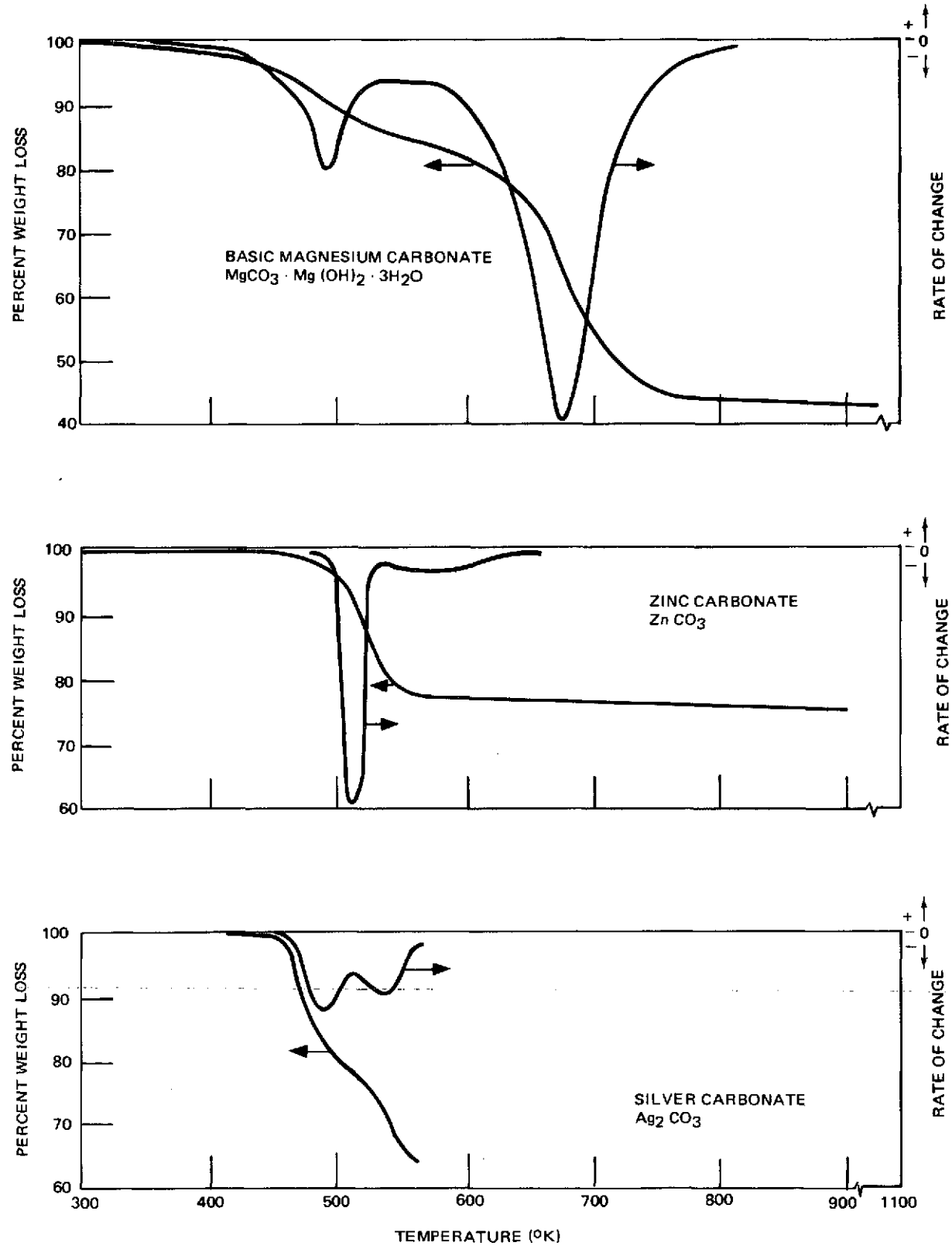

Figure 2-19. Thermogravimetric Analyses of Reagent Grade Carbonates

distinct decompositions, probably $Mg(OH)_2$ and H_2O at 500°K and then $MgCO_3$ around 675°K. Zinc carbonate shows one fairly sharp decomposition just above 500°K. The curves for silver carbonate show two decompositions and the percent lost is greater than theoretical for going to the oxide. Apparently the oxide decomposition to metallic silver begins near 500°K.

Figure 2-20 shows the same TGA for pure silver carbonate and a differential thermal analysis (DTA) curve. The DRA shows the energy requirement as the decomposition progresses. The phase change near 470°K, reported by Culbertson in Reference 5 is not distinguishable from the large decomposition peak unless one assumes the small humps on the large peak to be meaningful. The smaller hump appearing as 550°K is approached probably indicates the onset of Ag_2O decomposition.

The decomposition of compound S4 was studied in several environments as shown in Figure 2-21. A comparison of S4 in argon with pure silver carbonate shows a very different process. The very early decomposition correlates with the early peaks observed during the large-scale regenerations. The decomposition to Ag_2O appears to stabilize after 525°K as evidenced by the rate returning to zero. Complete decomposition in the vacuum test appears to require higher temperatures for completion. However, it is probable that this is an instrumentation error since the thermocouple was shielded from the furnace wall by the sample holder and relied on secondary radiation for its energy. In gaseous environments, the thermocouple received its heat by conduction and probably came closer to matching the specimen temperature. The lower curve shows the effect of CO_2 partial pressure compared with the test run in argon. Complete decomposition did not occur until 600°K; however, it appears to have stabilized as the oxide even at this temperature.

Figure 2-22 shows a TGA of S4 carried to completion. The two-peak carbonate decomposition is followed by a multipeak decomposition of the oxide to the metal. Appreciable decomposition of the oxide does not appear to occur until 600°K.

Figure 2-23 shows the sorption process of compound S4 as measured in the TGA apparatus. The upper curve is from the sample that was decomposed

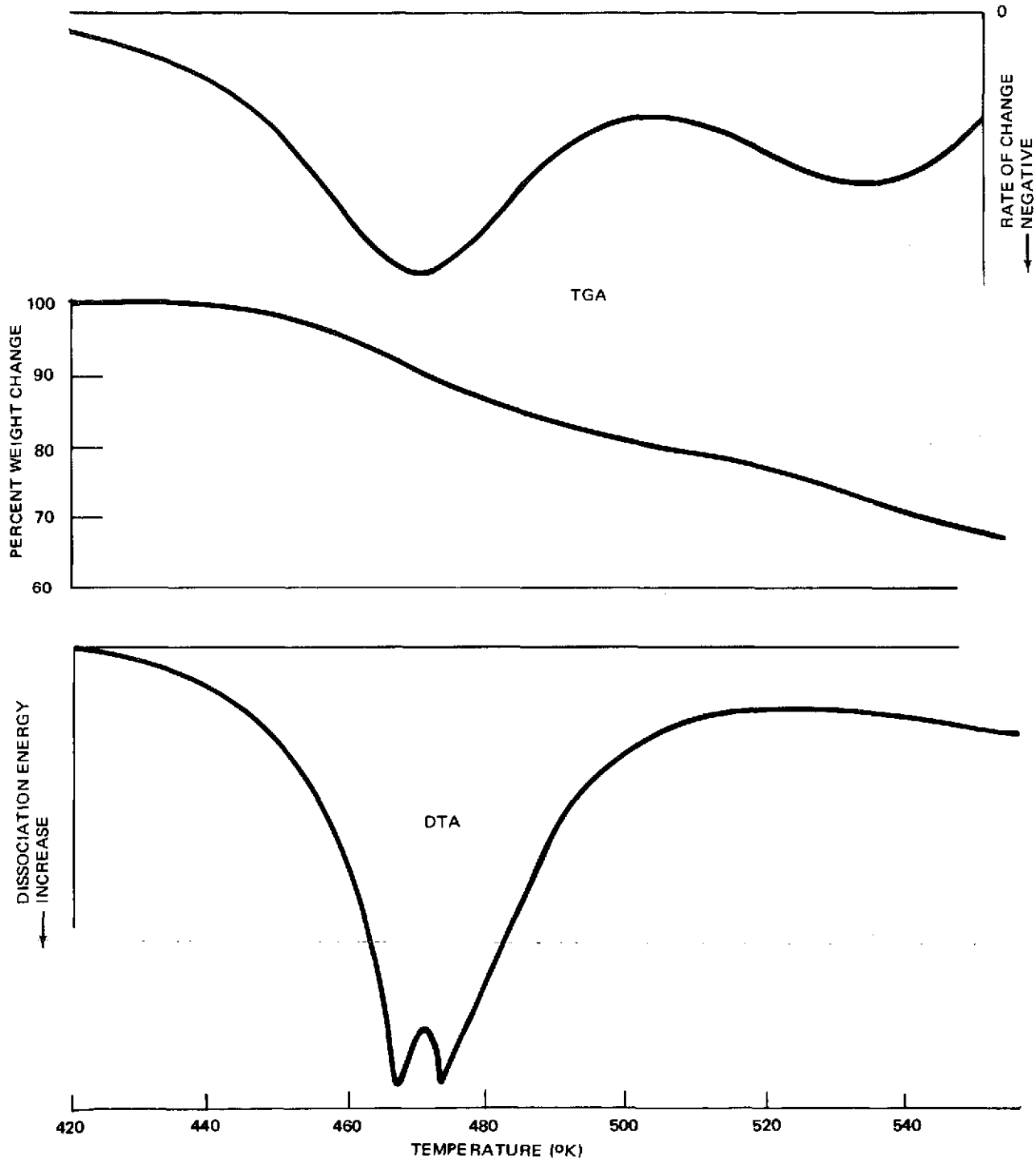

Figure 2-20. Thermogravimetric Analysis (TGA) and Differential Thermal Analysis (DTA) of Reagent Grade Silver Carbonate

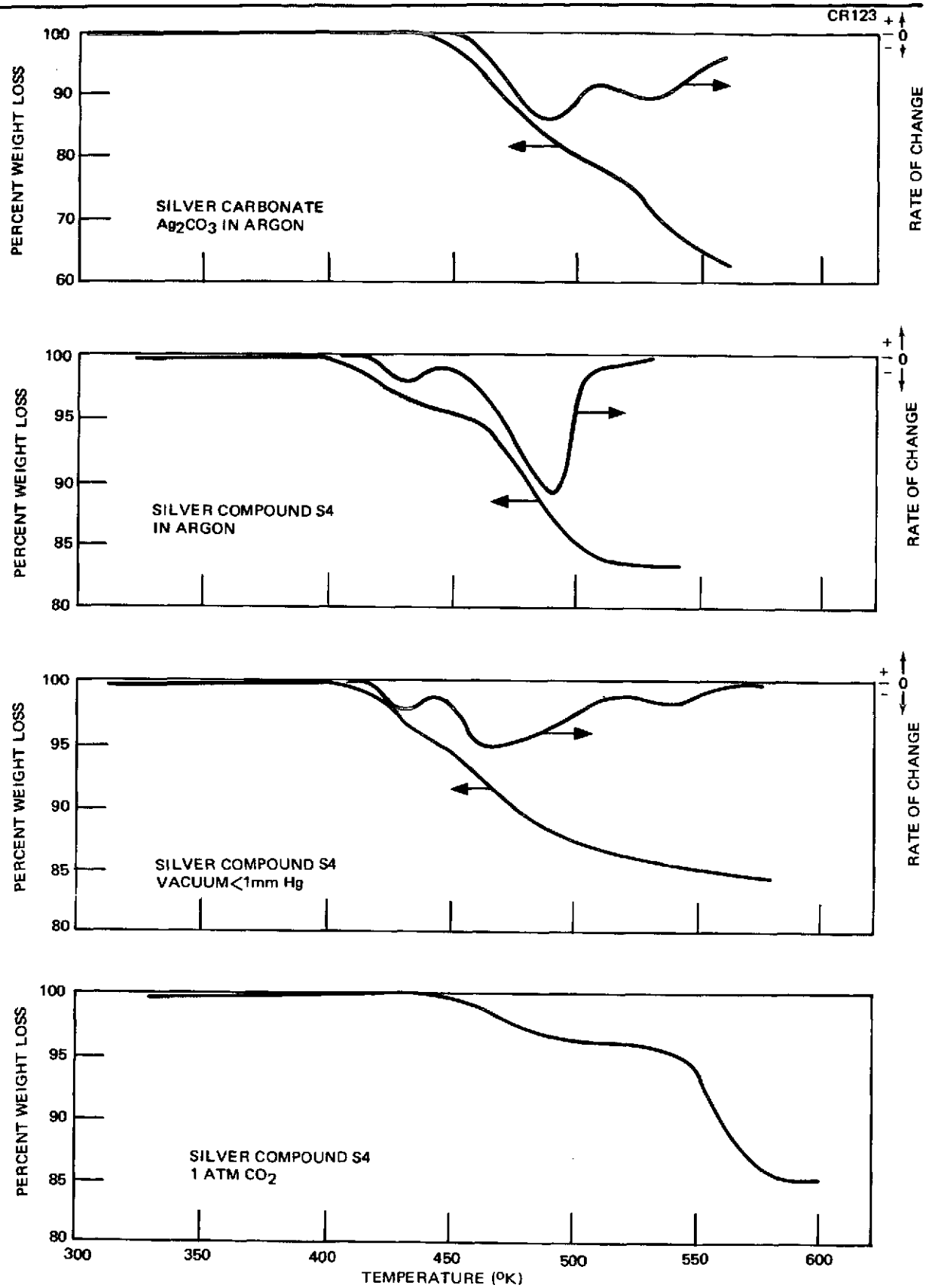

Figure 2-21. Thermogravimetric Analyses of Silver Carbonate and Compound S4

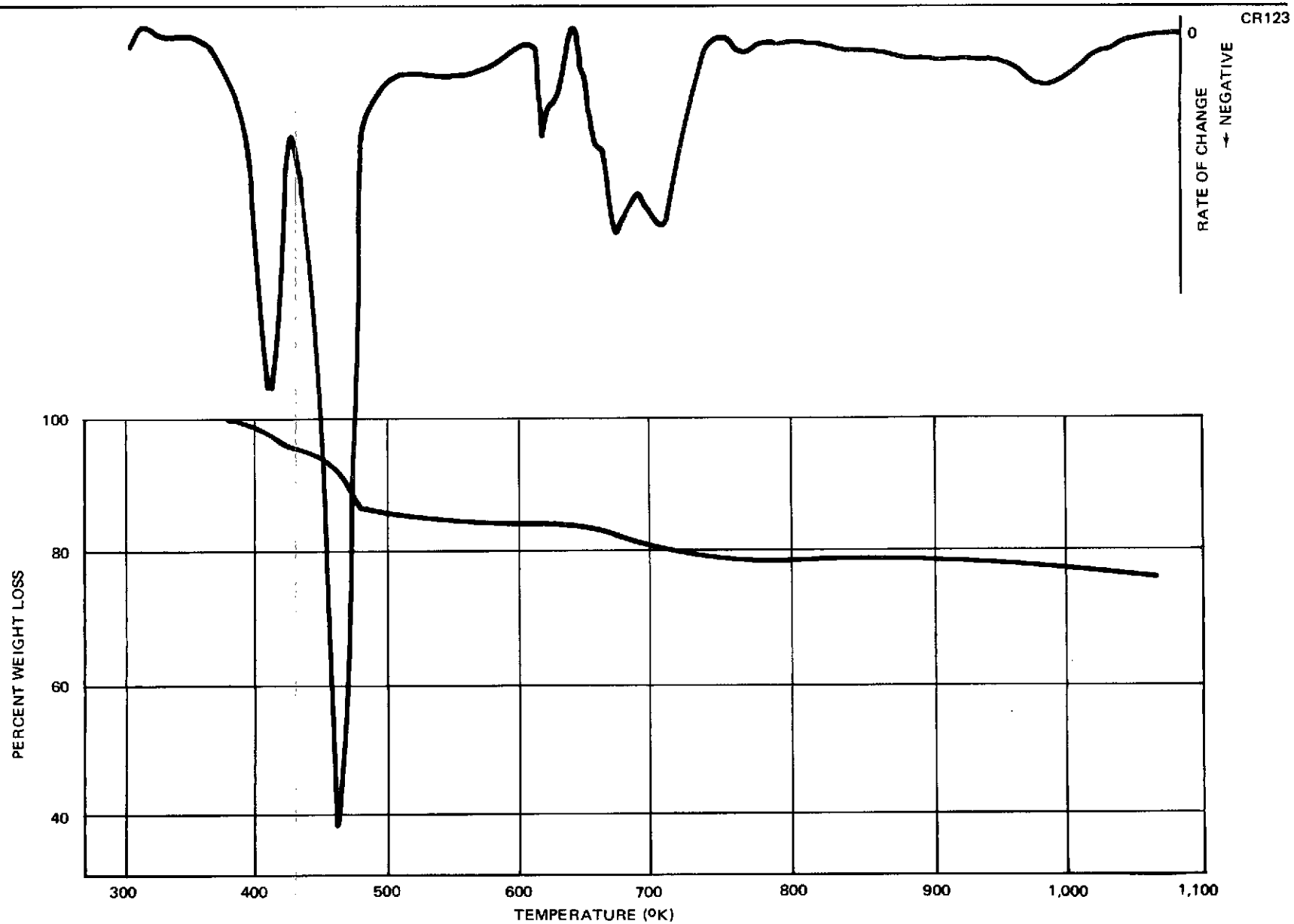

Figure 2-22. Thermogravimetric Analysis of Compound S4 to 1,100°K

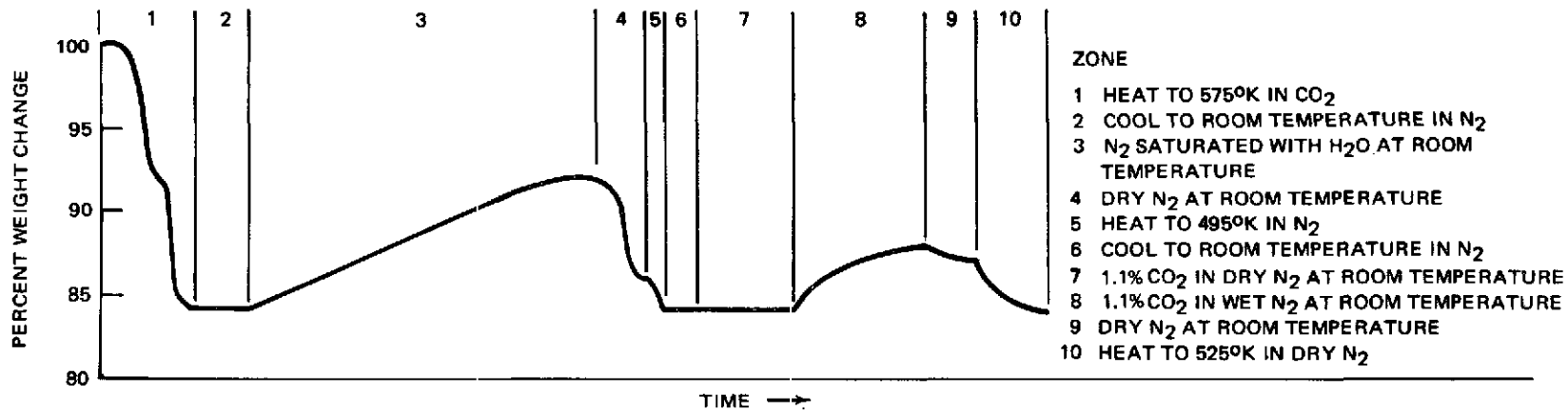

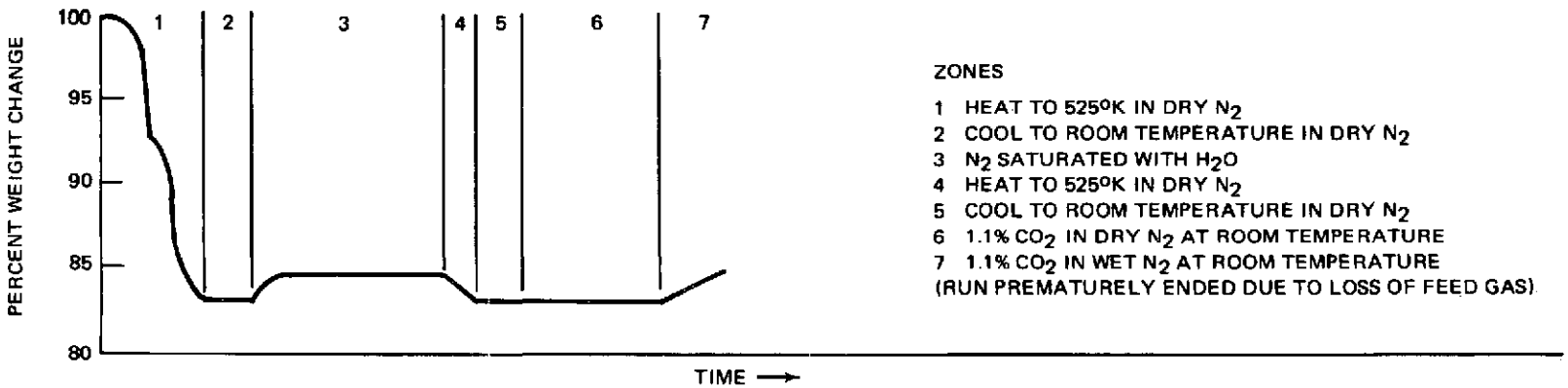

Figure 2-23. Thermogravimetric Analysis of Compound S4, Regeneration and Sorption

in CO_2 up to 575°K. After cooling to room temperature in dry N_2, a water-saturated stream of N_2 was admitted to the system. Moisture adsorption occurred at a fairly rapid rate. However, switching back to dry N_2 quickly removed the bulk of the moisture, indicating adsorption, and the rest was quickly removed by heating to 475°K. After cooling, 1.1 percent CO_2 in dry N_2 was admitted to the system. No sorption of CO_2 was evident. The addition of moisture to the stream caused an immediate weight gain; however, it is not clear whether CO_2 or water was being taken up. Passing dry N_2 again only removed a small portion thus suggesting CO_2 sorption or possibly both assuming the K_2CO_3 - $KHCO_3$ reaction. Reheating to 525°K brought the sample back to the minimum weight.

The lower curve in Figure 2-23 shows a fresh sample that was regenerated up to 525°K and cooled in dry N_2. Saturating the N_2 stream with water caused only a small gain in weight compared to the previous sample. Apparently, a significant change in the surface of the previous material was caused by heating to 575°K in pure CO_2. In the second sample, after driving the water off at 525°K and cooling, 1.1 percent CO_2 in dry nitrogen caused no detectable weight gain. Humidifying the stream again showed an immediate weight gain. Unfortunately, the tank of feed gas became empty thus prematurely terminating the test. The two tests did, however, show a significant effect on the moisture sorption characteristics.

Figure 2-24 shows a series of TGA sorption tests conducted with a freshly manufactured pellet of compound S7. The regeneration of the new pellet showed only an 11 percent weight loss compared to the 16 percent observed with the older S4 sample. Sorption in wet 1.1 percent CO_2 in N_2 proceeded essentially back to 100 percent in the time alloted. The next regeneration went down to the same weight; however, dry 1.1 percent CO_2 in N_2 produced a 5 percent weight gain and then stabilized. Humidifying the stream and running over a weekend brought the weight back to 100.7 percent of original. The next regeneration and sorption shows a much higher rate in the early phase and 100% was achieved in a relatively short time. Thus, the rate and capacity increasing over the first two or three regenerations is observable here also.

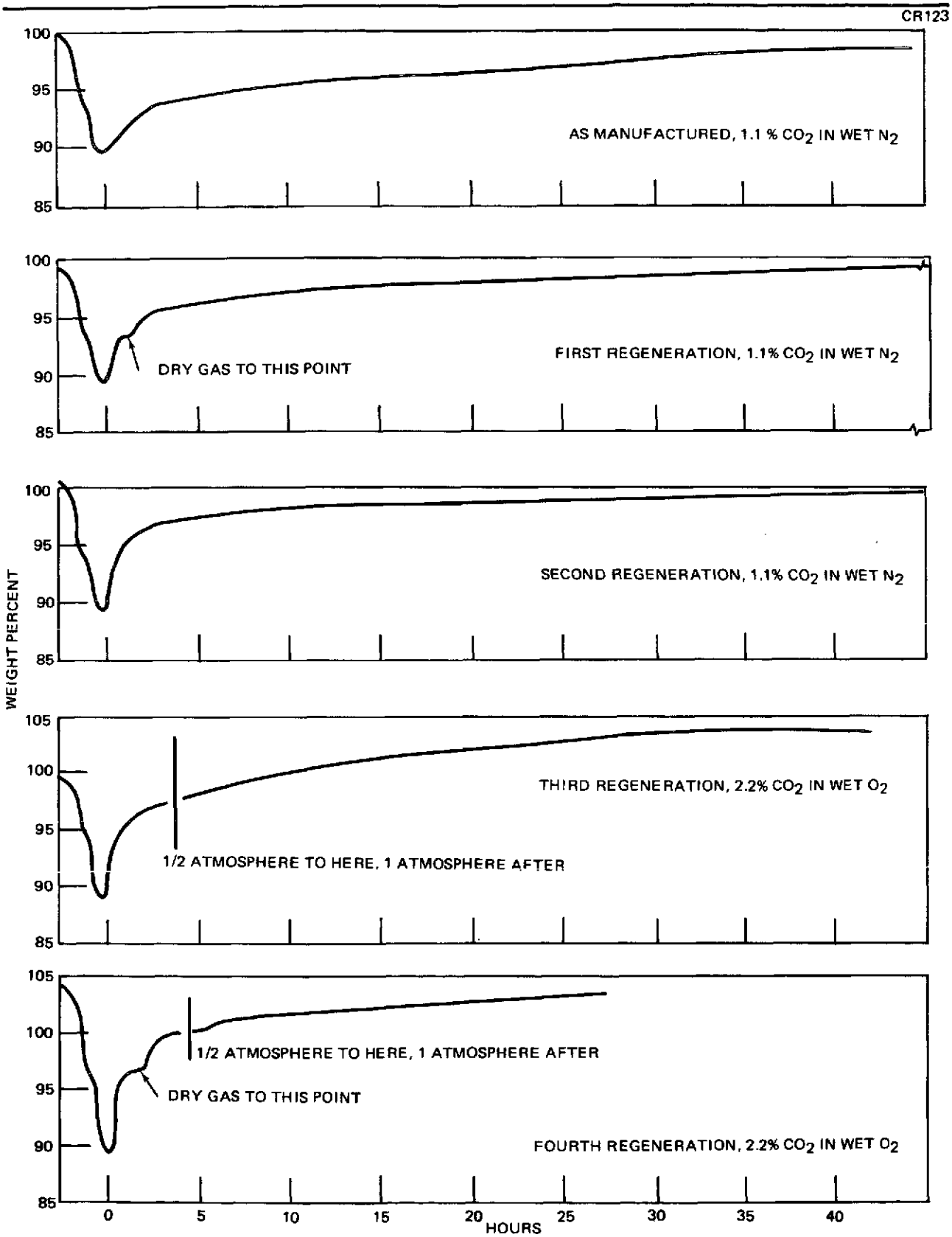

Figure 2-24. Thermogravimetic Analysis of Compound S7
(Heating to 525°K in Dry N_2 Followed by Cooling to Room Temperature up to Time Zero)

The fourth curve shows an attempt to duplicate actual AEPS conditions, i.e., pure oxygen at low pressure. A very rapid sorption was observed which went to 104 percent. This is probably explained by the fact that the partial pressure of CO_2 was twice that of the previous tests for the latter part of the test. The fifth curve shows rapid sorption initially with dry gas, improvement with the addition of moisture, and rapid completion with the increase in CO_2 partial pressure. Thus, these two tests demonstrate compatibility with projected AEPS atmospheres and a possible improvement in sorption rates over the previous test conditions.

2.5.2 Physical Properties of Pellets

The surface and porosity characteristics of the best magnesium and silver pellets were measured. The surface areas were measured by the BET method. This involves the deposition of a monomolecular layer of nitrogen molecules on the surface and then measuring the amount of gas as it is given off. Porosity measurements were made by mercury intrusion porosimitry. In this process, the amount of mercury forced into the pores at a given pressure is used to calculate pore volume as a function of pore diameter. At the same time, the apparent density of the pellet is determined by measuring the volume of mercury displaced by a given weight of pellets at zero pressure.

Table 2-12 presents the surface area, percent open porosity, and apparent density of various forms of compound S7 and M7. Compound M7 is a new batch of pellets of composition identical to the best magnesium compound tested, M6. The specific area data for the S7 samples is somewhat unexpected since the area of S7D4 oxide is less than S7D1; this in spite of the fact that S7D4 showed better sorption characteristics than S7D1. In addition, the area of the S7D4 carbonate is greater than the oxide in spite of a significantly lower open porosity and higher apparent density. However, since the areas are all within 10 percent of an average (the level of precision expected as reported in Reference 6), the differences may be ignored as experimental error.

Figure 2-25 shows an increase in porosity from S7D1 to S7D4, as would be expected from sorption tests, with an attendant decrease after exposure to CO_2.

Table 2-12

PHYSICAL PROPERTIES OF PELLETS

Compound	Area[1] m^2/mKg	Percent Open Porosity[2]	Apprent Density $Kg/m^3 \times 10^{-3}\left(\frac{gm}{cc}\right)$[2]
S7D1 oxide	3.31	67.16	1.8590
S7D4 oxide	3.02	70.37	1.8719
S7D4 carbonate	3.41	53.88	2.0810
M7D oxide	17.8	80.68	0.5475
M7W oxide	8.4	68.05	0.8081
M7DW5 oxide	6.8	-	-
M7W carbonate	-	59.73	0.9920

(1) As measured by BET method.

(2) As measured by mercury intrusion porosimitry.

The areas and porosities of the M7 compounds are considerably greater than those of the silver compounds. The addition of water causes a large loss in area although it greatly enhances the CO_2 sorption properties of the material. Figure 2-25 also shows a large decrease in porosity from M7D to M7W. A further decrease in porosity after sorption of CO_2 is also evident.

2.5.3 Scanning Electron Microscope Studies

Detailed photographs of the surfaces and fractured cross sections of various pellet configurations were obtained using a scanning electron microscope. Samples were prepared by vacuum depositing a thin layer of gold on the pellets to provide an electrically conductive surface.

Figure 2-26 shows the surface of an M7W pellet in both the oxide and carbonate form. The oxide form shows a very porous, granular structure. The rod-shaped forms are the asbestos fibers added as a binder. The carbonate form shows a number of spiny-appearing clumps on the surface. These are shown at a higher magnification in Figure 2-27. The clumps are actually made up of fine plates of carbonate which have grown from the surfaces of

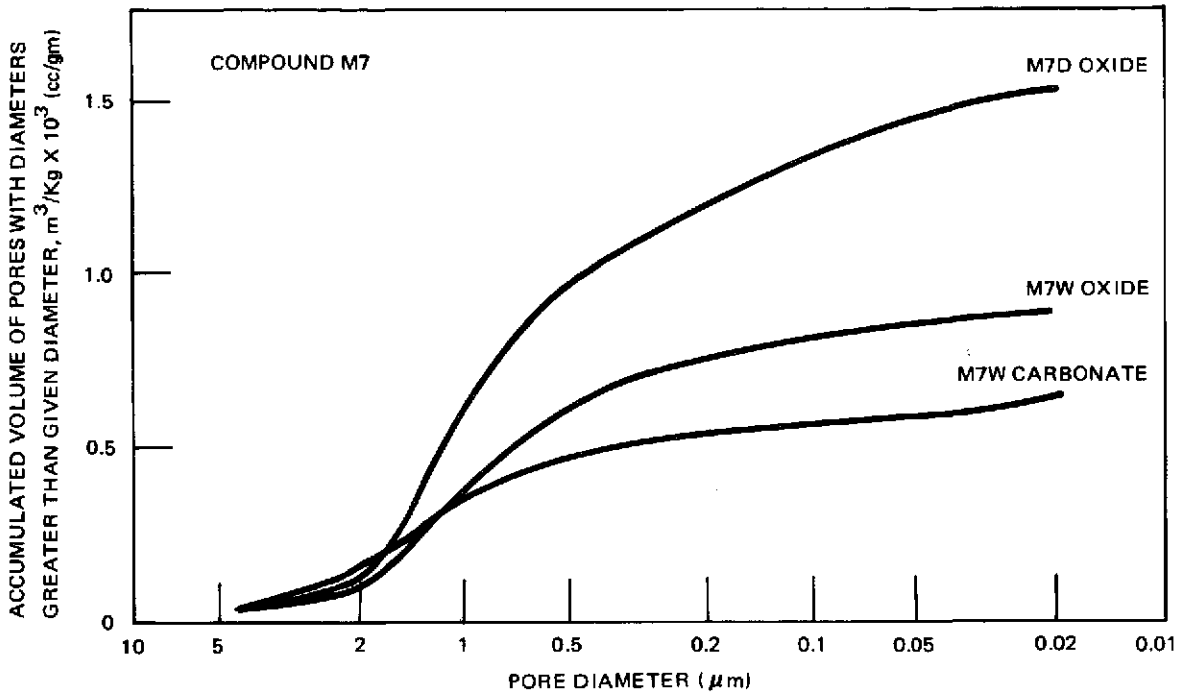

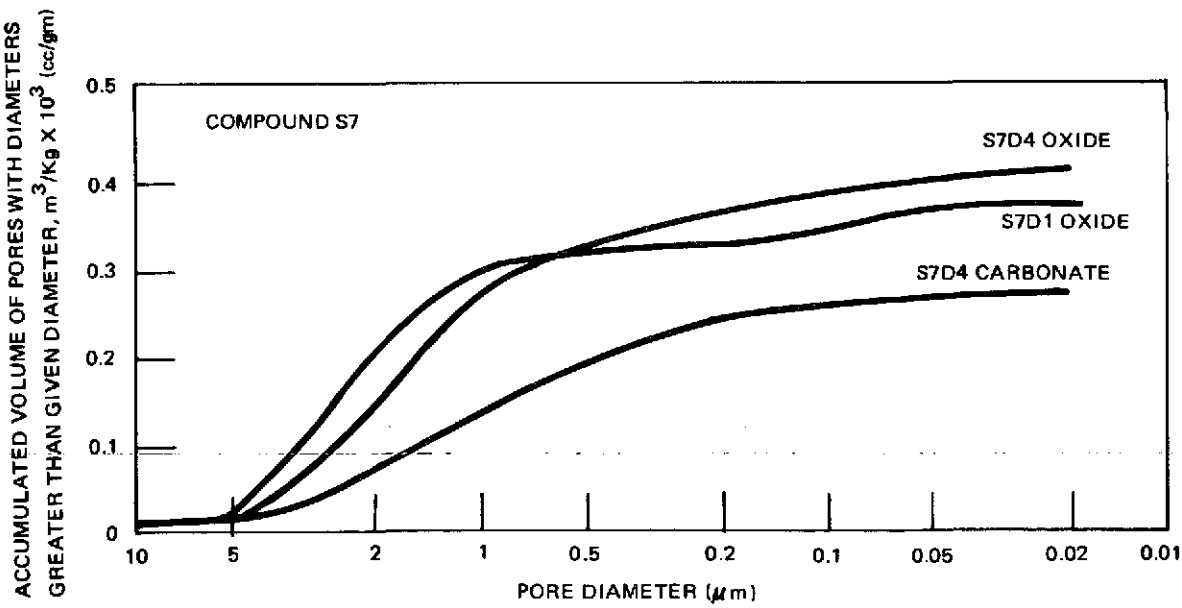

Figure 2-25. Pore Size Distributions

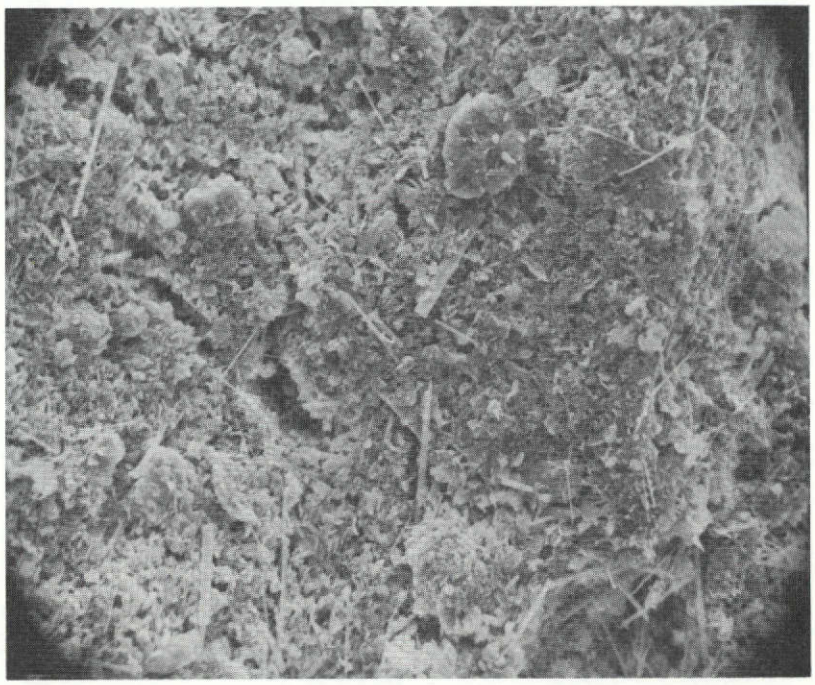

Oxide Form 500X

Carbonate Form 500X

Figure 2-26. Surface of Sample M7W

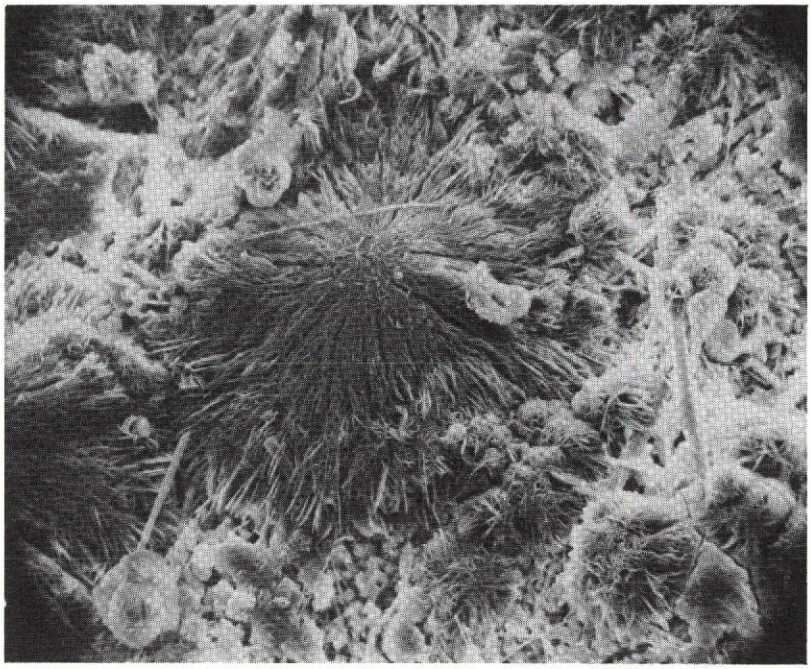

500X

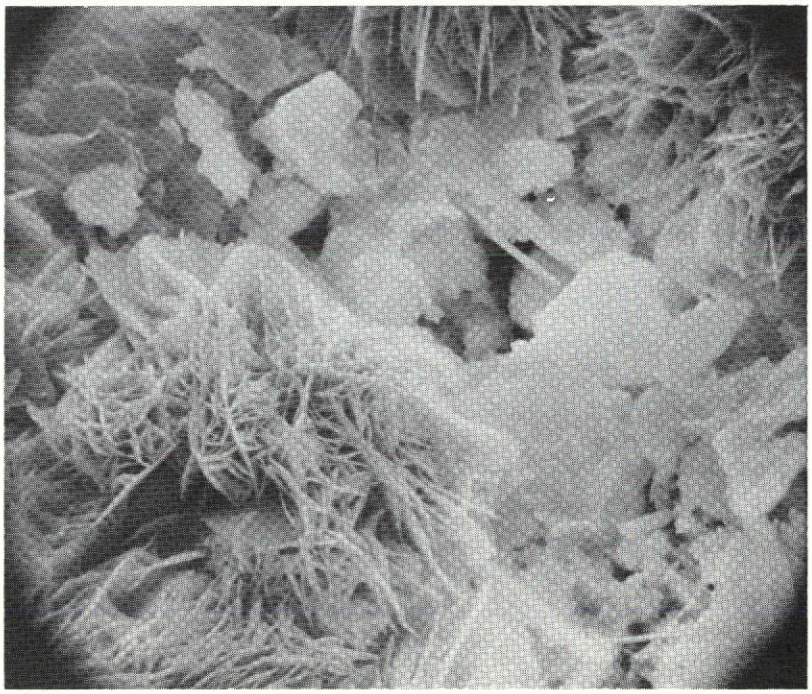

2,000X

Figure 2-27. Surface of Sample M7W in Carbonate Form

some of the oxide particles. Energy-dispersible x-ray analysis of these clumps show them to contain a higher potassium content than the granular particles and essentially no silicon. Thus, it appears that these carbonate growths are selectively concentrating the potassium, and repeated regenerations will eventually lead to a separation of the active ingredients. This will eventually lead to loss of activity and/or structural integrity. Additional photographs are shown in the appendix.

Figures 2-28 and 2-29 show the surface of compound S7 after 1, 4, and 12 regenerations. A definite change is taking place; however, the material remains a porous yet amorphous structure. The lower photograph shows the surface of S7D12 in the carbonate form. The carbonate seems to grow throughout the structure and retains its amorphous properties. This is ideal behavior for a regenerable system since no localized changes take place. Figure 2-30 shows cross sections of the interiors of two pellets. A change has again taken place but the structure remains continuous. Cross sections of carbonate forms, shown in Figure 2-31, show an almost glassy continuity in the structure while maintaining some open structure. Figure 2-32 shows high-magnification views of an oxide and carbonate surface. It appears from the carbonate surface pictures in Figures 2-29 and 2-32 and the cross sections in Figure 2-30 that a carbonate skin forms on the pellets. It appears to be quite impervious and one would expect it to form early in the sorption process and hinder complete utilization of the pellet. However, sorption data show greater than 90-percent theoretical conversion with good sorption rates. Therefore, either the skin has sufficient holes, including those that are not obvious, to permit good mass transfer, or solid diffusion in the matrix is very rapid. The relatively low surface area of this material — 3 m^2/mKg compared to common adsorbents such as molecular sieves — suggests that solid diffusion is likely the dominent mechanism. Additional cross section views are shown in the appendix.

Figure 2-33 shows the surface of a zinc oxide pellet. The light rod-shaped structures are assumed to be zinc carbonate formed by exposure to the air during sample handling. The profusion of these structures on the surface of the carbonate form, Figure 2-34, indicates that zinc carbonate grows from particles in a manner similar to that of magnesium carbonate and thus will eventually lead to selective separation of components. Cross sections of the

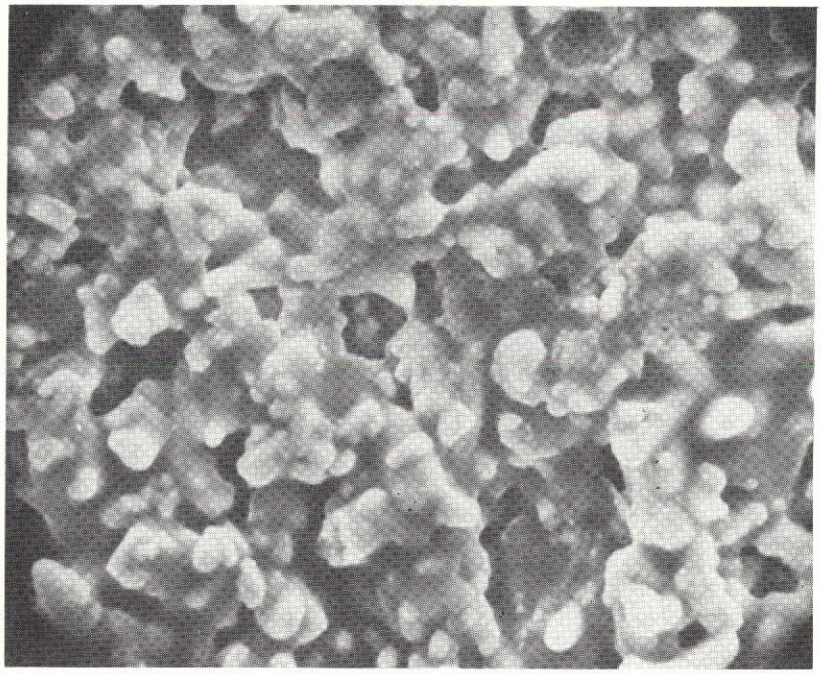

S7D1 2,000X

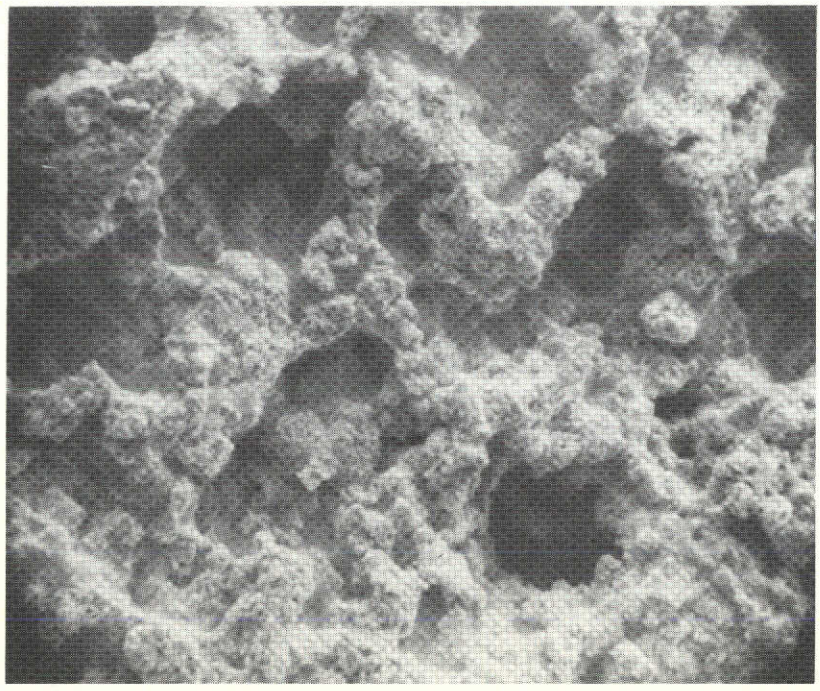

S7D4 2,000X

Figure 2-28. Surface of Sample S7D Oxides

oxide and carbonate forms shown in Figures 2-35 and 2-36 show an absence of the rod-shaped structures evident on the surface; this indicates that the reaction is limited to the surfaces of the pellets and somewhat explains the poor sorption performance of the zinc compounds.

2.6 DISCUSSION OF RESULTS

The objective of this program was to select the most promising candidate for development into a regenerable CO_2 sorbent for EVA. The first conclusion that may be drawn is that magnesium and zinc hydroxides may be eliminated from further considerations. Since the hydroxides decompose at a temperature lower than the carbonates, regenerability is impossible since the oxides do not rehydrate. In addition, the hydroxides showed little affinity for CO_2. This also discounts the previously assumed mechanisms which involved the hydroxides as intermediates when wet oxides react with CO_2.

The potential development of zinc oxide is also doubtful based on the results discussed earlier. All sorption capacities are quite low, based on theoretical analysis, and the binder which was successful with other materials was ineffective with zinc oxide compounds. In addition, SEM studies indicate the selective separation of materials during the carbonation reaction thus eventually limiting regenerability.

Magnesium oxide compounds, although theoretically having the highest sorbent capacity, could not be induced to absorb CO_2 beyond approximately 15 weight percent. In addition, they require the highest regeneration temperature and must be pre-wetted before they become active. A binder system was developed which yielded very strong stable pellets. The SEM photographs show a granular consistency with the carbonate growing away from the particle surfaces. This process was found to selectively concentrate the catalyst in the carbonate and reject the binder. Repeated regenerations will obviously lead to decomposition of the structure.

The results from the tests of silver oxide compounds are most encouraging. Compounds S4 and S7, with identical compositions, were found to absorb essentially 95% of their theoretical capacity through 28 regenerations without any noticeable loss of efficiency. Although the weight percent attained is

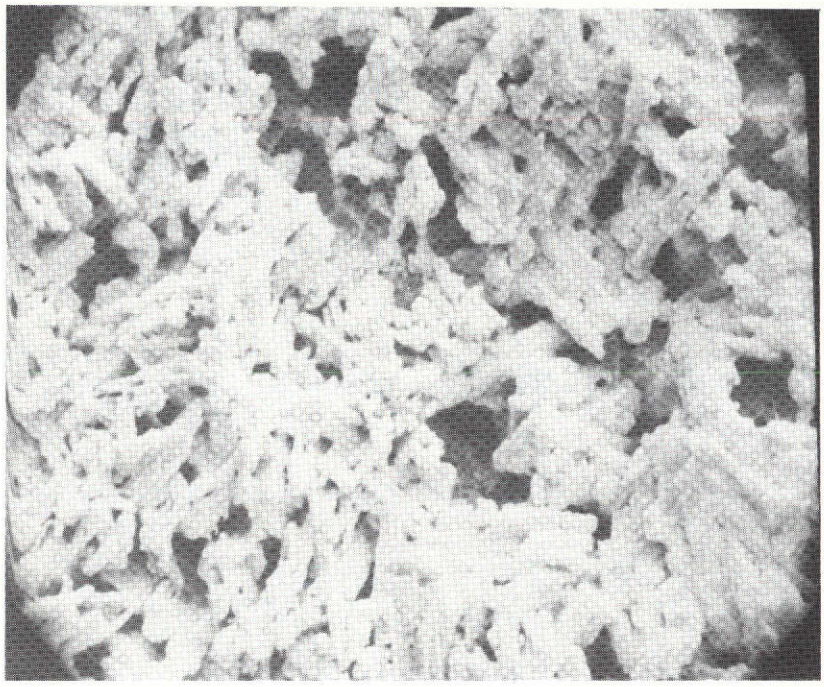

Oxide 2,000X

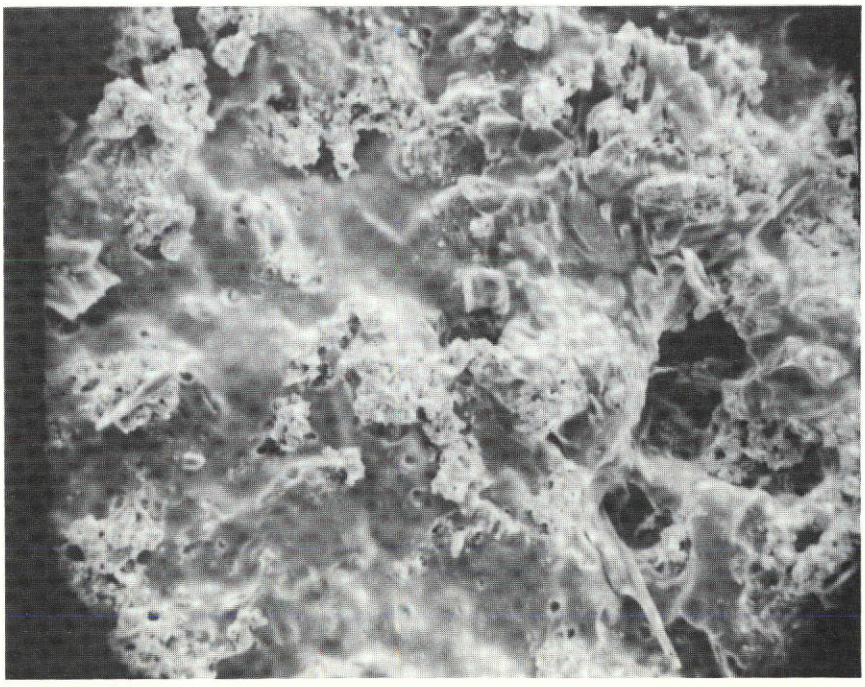

Carbonate 2,000X

Figure 2-29. Surface of Sample S7D12

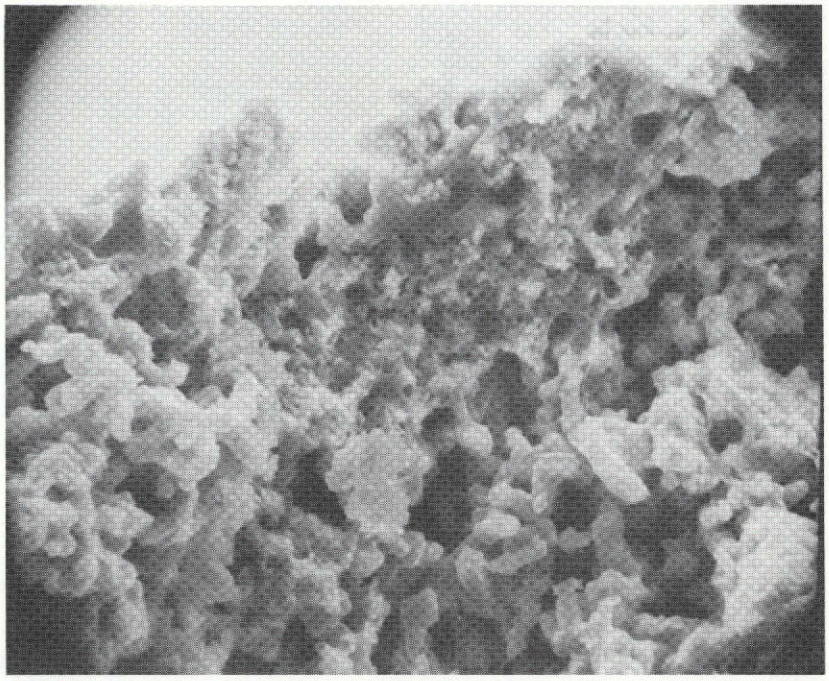

S7D1 2,000X

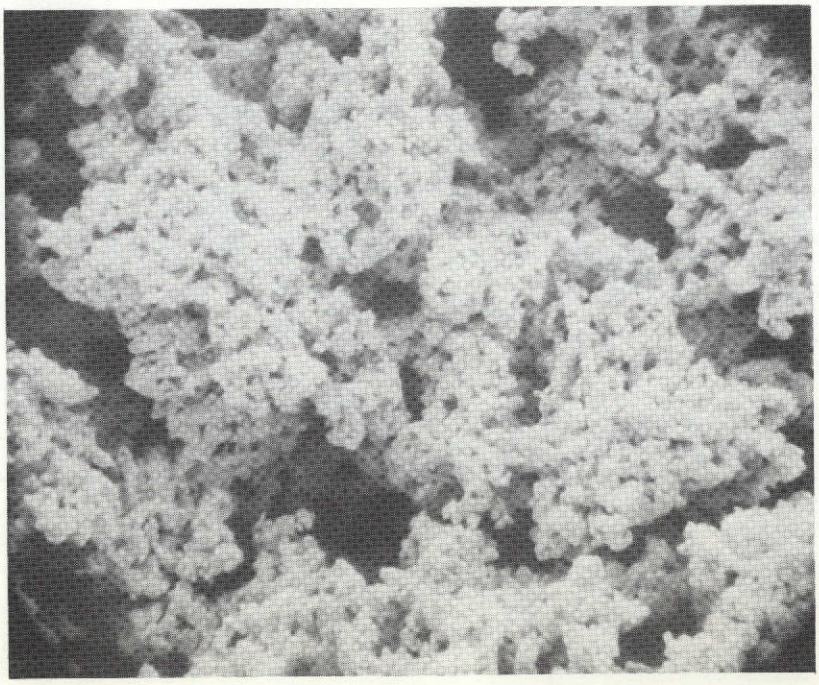

S7D4 2,000X

Figure 2-30. Cross Sections of Sample S7D

500X

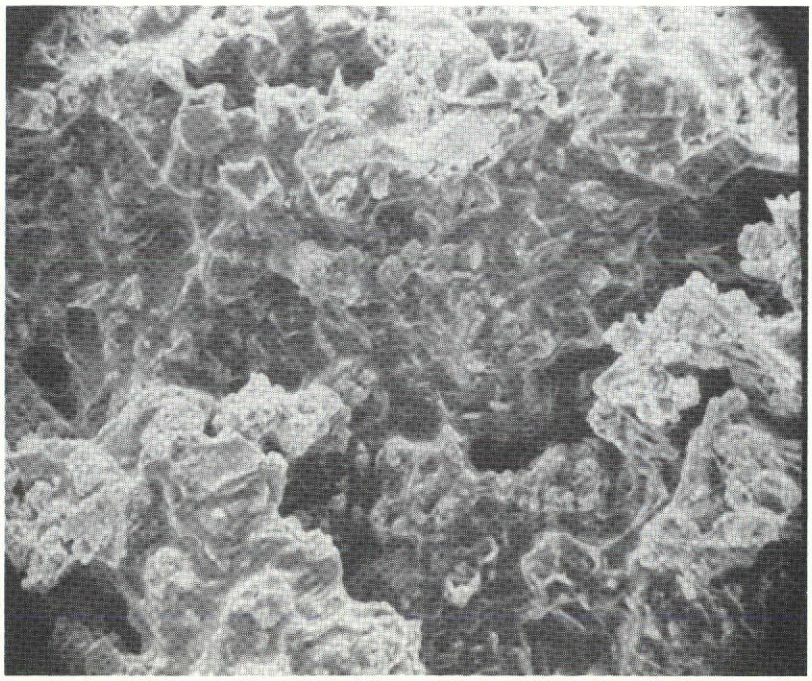

2,000X

Figure 2-31. Cross Sections of Sample S7D12 in Carbonate Forms

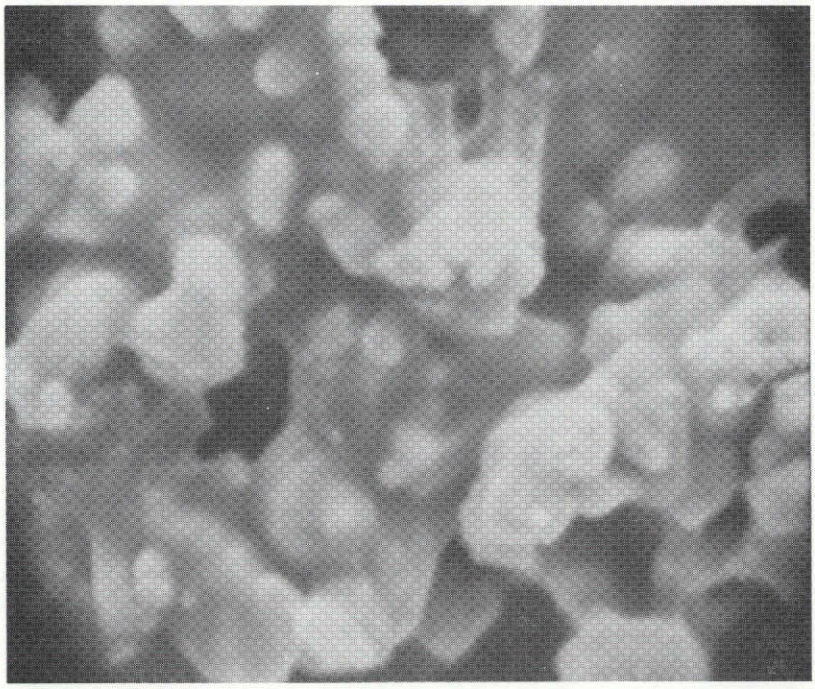

S7D1, Oxide Form 5,000X

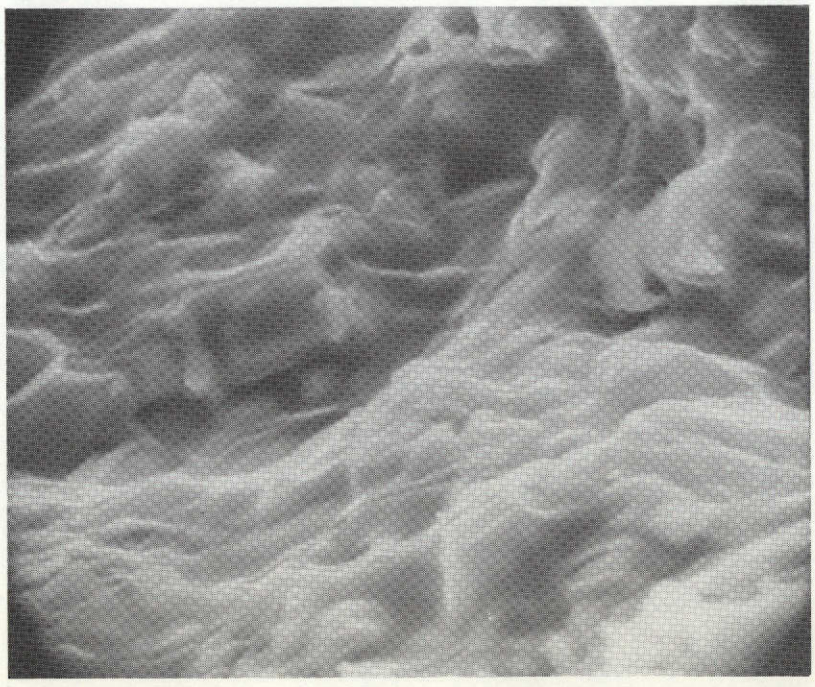

S7D4, Carbonate Form 5,000X

Figure 2-32. Surface of Sample S7D

approximately the same as attained in some of the better magnesium oxide compounds, the density differences between silver oxide and magnesium oxide makes silver oxide much more efficient based on volume requirements. In addition, the regeneration temperature for silver oxide is much lower and no pre-wetting is required. Silver oxide is clearly the most promising candidate of the five materials specified in the contract for further development.

The studies presented above, in addition to communications with other investigators working in the area, have led to a probable explanation of the role of potassium ion in the sorption process. During the manufacture of the silver compounds, a solution of KOH was added to the green Ag_2CO_3 powder. The powder immediately turned black, characteristic of Ag_2O. Since no gas evolved, it may be concluded that the KOH was converted to K_2CO_3. It has been observed that K_2CO_3 in the presence of moisture and CO_2 readily forms $KHCO_3$. The simultaneous breakthrough of water and CO_2, shown graphically in Figures 2-10, 11 and 12, indicate that this mechanism may be responsible for the high rates of CO_2 sorption in the early phases of the process. In addition, the early decomposition peak observed in the TGA tests with S4 and S7 corresponds closely to the decomposition temperature of $KHCO_3$.

A rough scale-up of the high flow breakthrough curves for S4 shown in Figure 2-9 was calculated in an effort to determine the bed size required for an actual AEPS. A direct proportional scale-up shows that 7.7 Kg of material will maintain the CO_2 partial pressure below 532 N/m^2 (4 mm Hg) for 10 hours at a metabolic rate of 1.3×10^6 J (1,200 Btu/hr.). The dimensions of this bed would be 0.18 m in diameter and 0.25 m long. This scale-up is very conservative since the feed concentration used in the test is the maximum allowable, and an actual system will start at zero and build up to that point. In addition, a larger bed will be more efficient due to increased depth and smaller wall effects. The Apollo LiOH cartridge weighs only 1.8 Kg. However, it is only rated for six hours and the maximum allowable CO_2 concentration is almost four times higher (Table 2-1). A LiOH cartridge sized to the AEPS specifications may not be much smaller than an AgO unit.

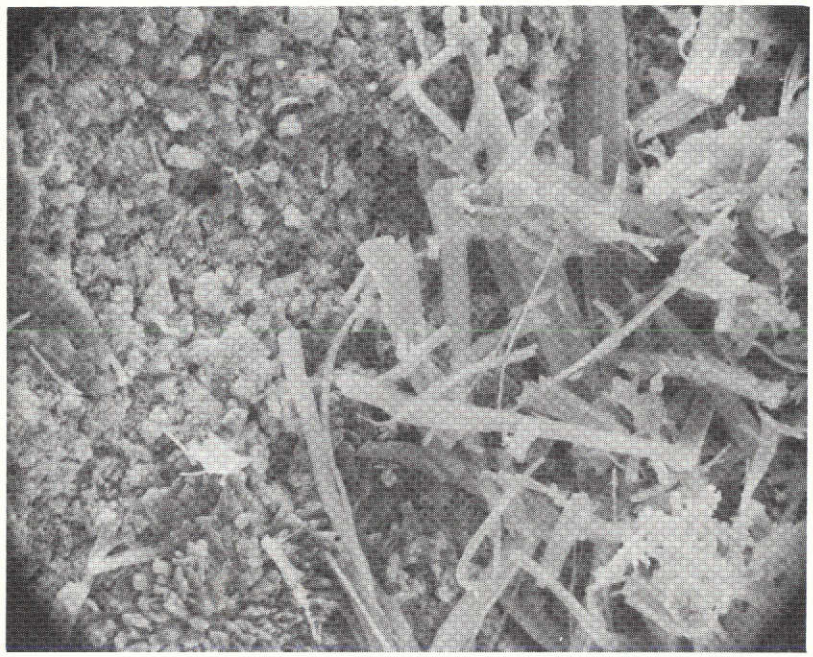

500X

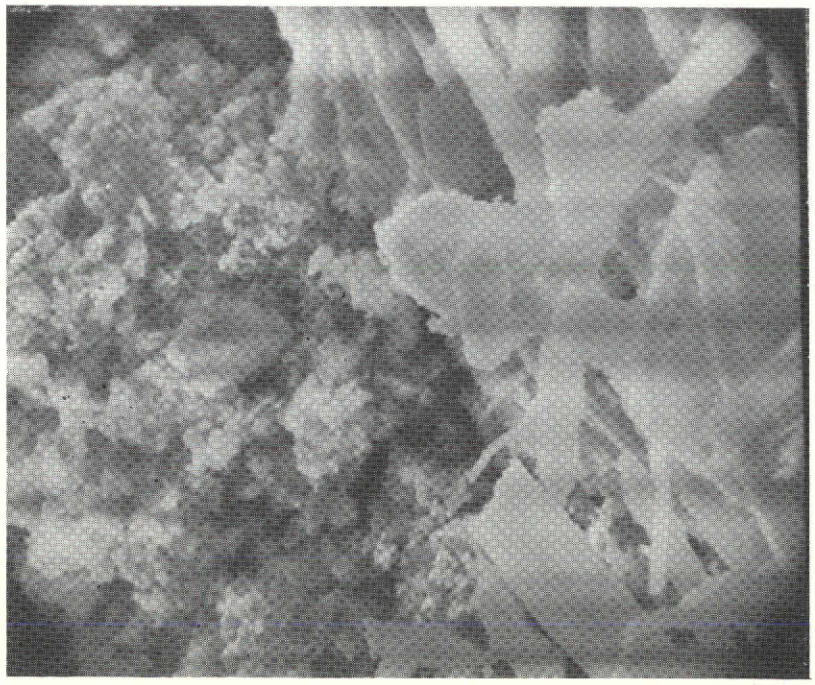

2,000X

Figure 2-33. Surface of Sample Z14D3W3, Oxide Form

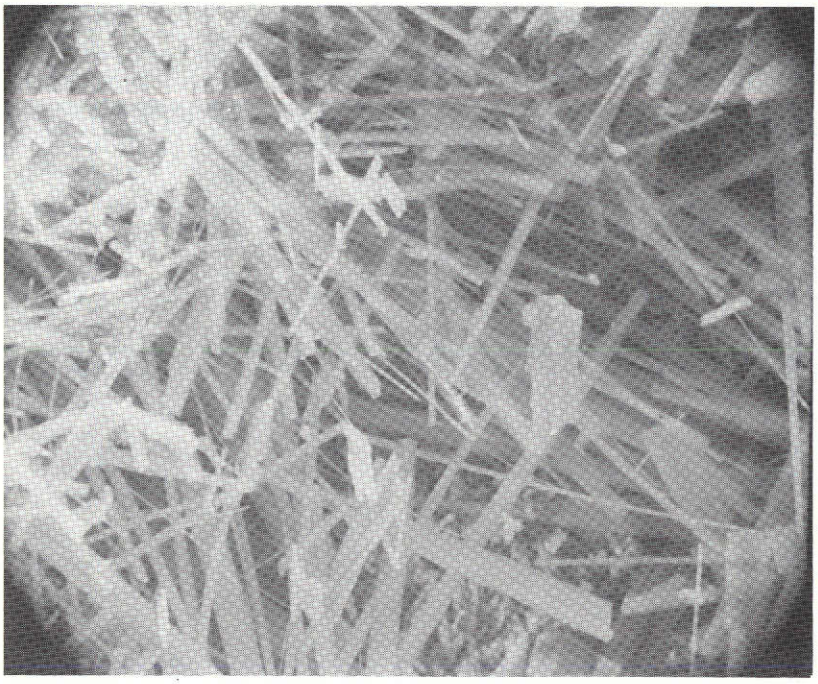

500X

2,000X

Figure 2-34. Surface of Sample Z14D3W3, Carbonate Form

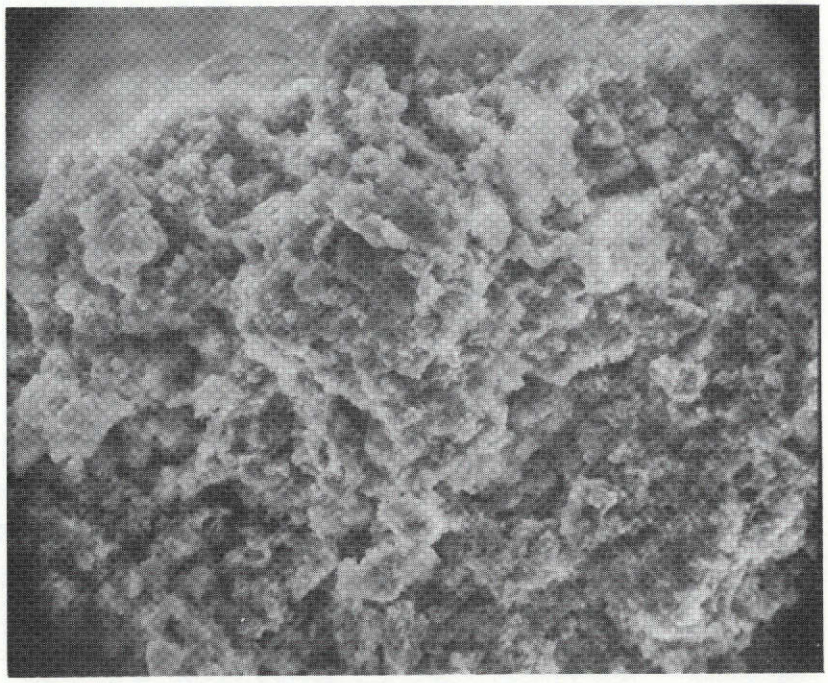

Oxide Form 500X

Carbonate Form 500X

Figure 2-35. Cross Section of Sample Z14D3W3

Oxide Form 2,000X

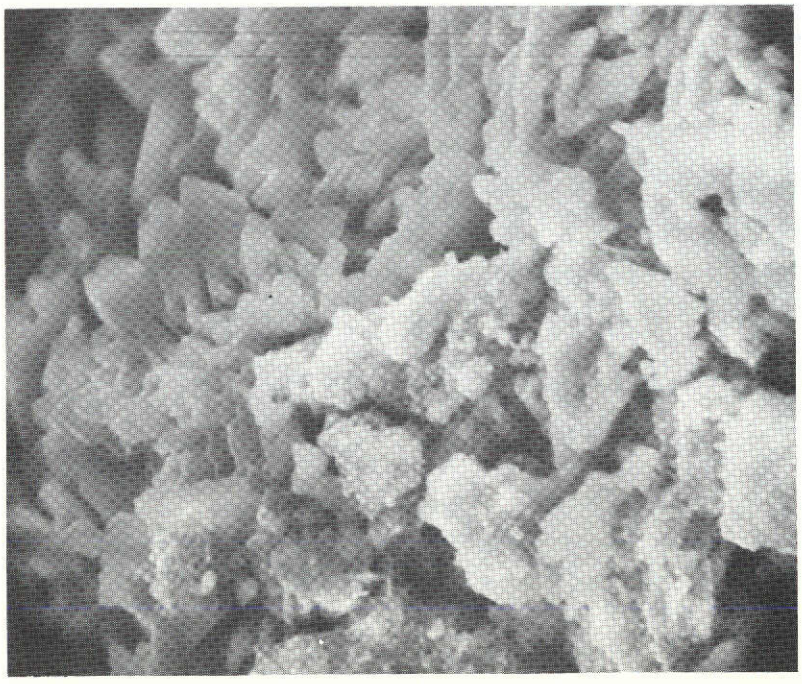

Carbonate Form 2,000X

Figure 2-36. Cross Section of Sample Z14D3W3

2.7 RECOMMENDATIONS FOR FURTHER DEVELOPMENT

It should be emphasized that the promising results with the silver oxide compound were obtained with the fourth composition tested. No attempts were made to optimize this compound. Systematic tests should be made in order to determine the effect of varying the relative concentrations of the various constituents.

Regeneration conditions were assumed to be responsible for the improved structural properties of S7 over S4. This phenomenon should be investigated in detail to define the conditions most conducive to long pellet life.

Large-scale tests should be conducted with a closed-loop system under the conditions expected in an AEPS to obtain data which can be used to accurately predict bed-size requirements and actual performance characteristics.

Although tests to date show that the silver oxide system has a high potential for successful development, it would be desirable to find a material with a higher CO_2 capacity. Table 2-13 lists five new metals whose carbonates decompose at a reasonable temperature and whose theoretical CO_2 sorption capacity is higher than silver oxide. These materials should undergo a cursory screening to ascertain their potential for further development.

Table 2-13

POTENTIAL METAL OXIDES FOR REGENERABLE CO_2 SORBER

Metal Oxide	Theoretical CO_2 Capacity (Kg CO_2/Kg oxide)	Theoretical Regeneration Temperature (^oK)
CoO	0.588	504
MnO	0.621	642
FeO	0.613	459
NiO	0.589	637
CuO	0.554	473

Section 3
CONCLUSIONS

- Magnesium hydroxide and zinc hydroxide show no potential for development into regenerable CO_2 sorbents.

- Zinc oxide shows a poor affinity for CO_2 and no satisfactory structural binder has been identified.

- A good binder system has been developed for magnesium oxide; however, the CO_2 capacity has not been improved over previous results.

- A silver oxide formulation has been developed which results in essentially theoretical CO_2 capacity at a high rate with good regenerability. This material should be developed further.

- Five new metal oxides have been identified whose properties suggest they should be tested to ascertain their potential for further development.

REFERENCES

1. Advanced Extravehicular Protective Systems (AEPS) Study, NASA Contract No. NAS2-6022, NAS CR-114321.

2. Advanced Extravehicular Protective Systems (AEPS) Study, NASA Contract No. NAS2-6021, NASA CR-114320.

3. G. V. Colombo and E. S. Mills. Regenerative Separation of Carbon Dioxide via Metallic Oxides. Chemical Engineering Progress Symposium Series, 1966; Vol. 62, No. 63, P 89-94.

4. J. C. Beggs and F. H. Goodwin. Apollo PLSS – Environmental Control of the Smallest Manned Space Vehicle. NASA Report No. SP-302, 1972.

5. W. J. Culbertson Jr. Investigation and Design of a Regenerable Silver Oxide System for Carbon Dioxide Control, AMRL-TR-64-119, 1964.

6. P. W. Jacobs and F. C. Tompkins. Surfaces of Solids, Chemistry of the Solid State. Butterworths Scientific Publications, London, 1955.

APPENDIX

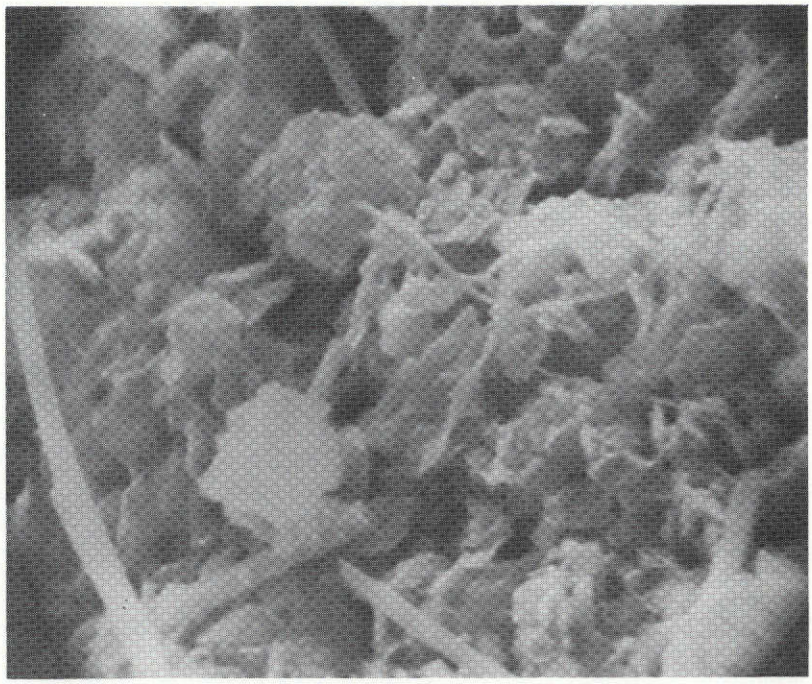

Oxide Form 5,000X

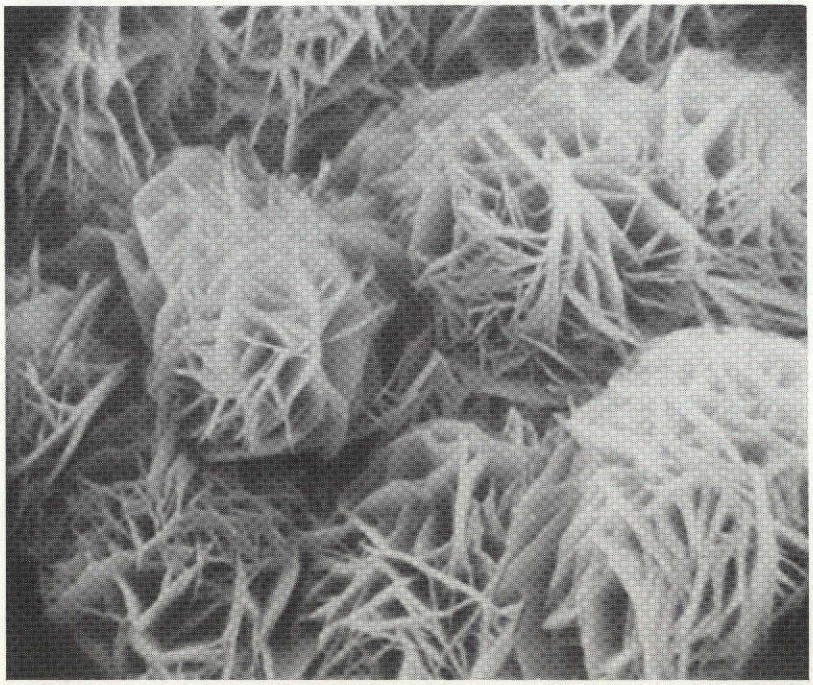

Carbonate Form 5,000X

Figure A-1. Surface of Sample M7W

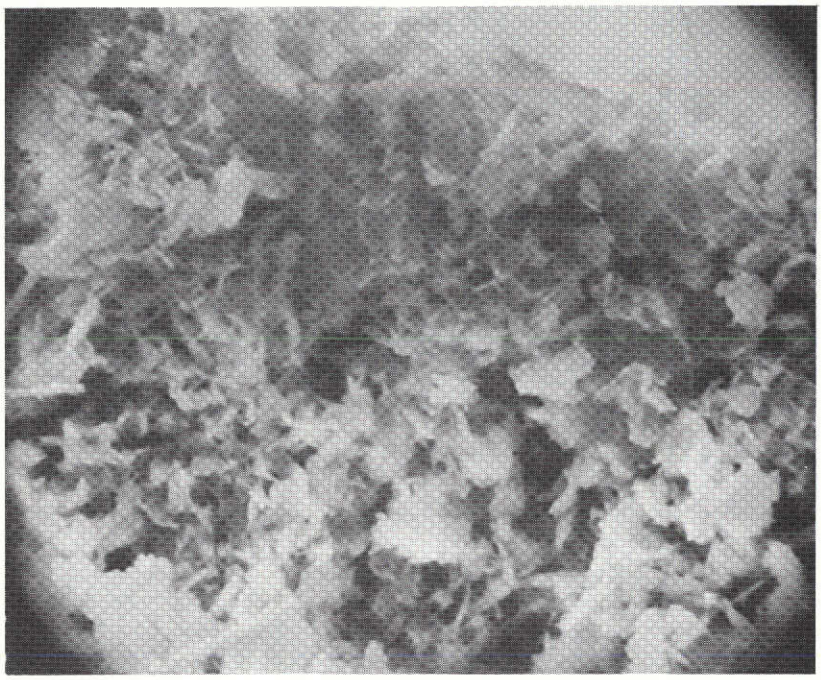

Oxide Form 2,000X

Carbonate Form 2,000X

Figure A-2. Cross Sections of Sample M7W

S7D1, Oxide Form 500X

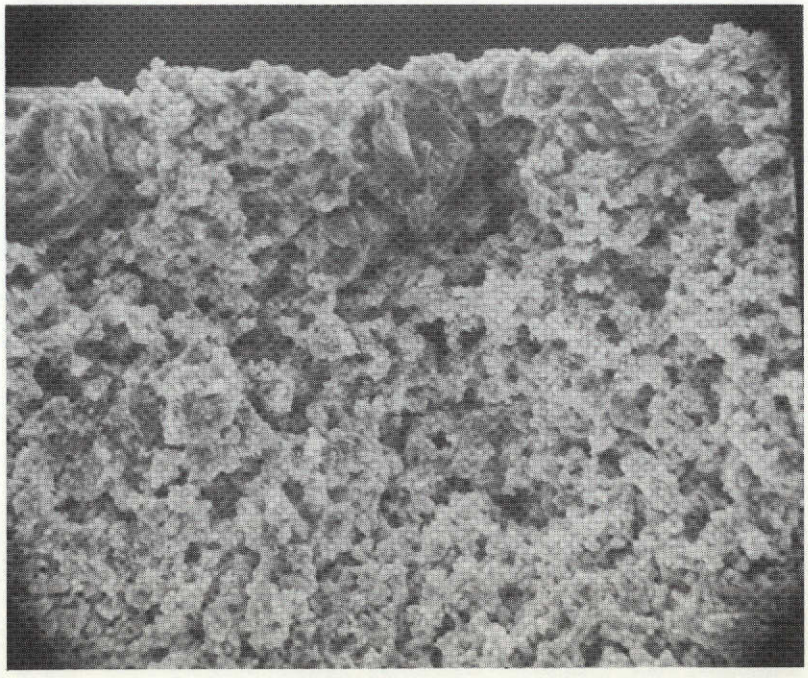

S7D4, Carbonate Form 500X

Figure A-3. Cross Sections of Sample S7D

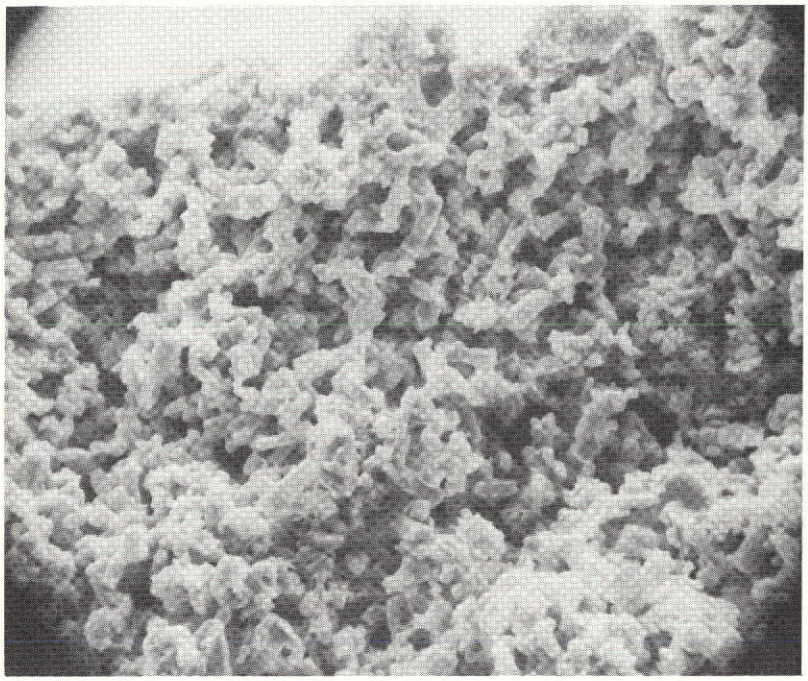

S7D1, Oxide Form 1,250X

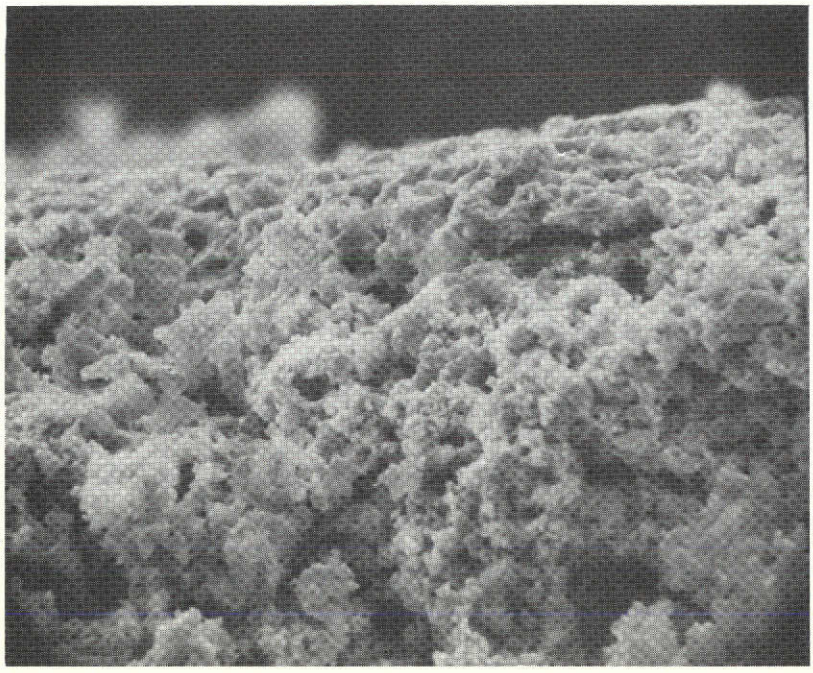

S7D4, Oxide Form 1,250X

Figure A-4. Cross Sections of Sample S7D